

Stephen F. Austin State University

SFA ScholarWorks

Electronic Theses and Dissertations

Fall 12-15-2018

Delineation of Karst Potential Using LiDAR and GIS Analyses, Fort Hood Military Installation, Texas

Colby Reece

colbyreece@rocketmail.com

Follow this and additional works at: <https://scholarworks.sfasu.edu/etds>



Part of the [Geology Commons](#)

[Tell us](#) how this article helped you.

Repository Citation

Reece, Colby, "Delineation of Karst Potential Using LiDAR and GIS Analyses, Fort Hood Military Installation, Texas" (2018). *Electronic Theses and Dissertations*. 226.

<https://scholarworks.sfasu.edu/etds/226>

This Thesis is brought to you for free and open access by SFA ScholarWorks. It has been accepted for inclusion in Electronic Theses and Dissertations by an authorized administrator of SFA ScholarWorks. For more information, please contact cdsscholarworks@sfasu.edu.

Delineation of Karst Potential Using LiDAR and GIS Analyses, Fort Hood Military Installation, Texas

Creative Commons License



This work is licensed under a [Creative Commons Attribution-Noncommercial-No Derivative Works 4.0 License](https://creativecommons.org/licenses/by-nc-nd/4.0/).

Delineation of Karst Potential Using LiDAR and GIS Analyses

Fort Hood Military Installation, Coryell County, Texas

By

Colby Reece, Bachelor of Science

Presented to the Faculty of the Graduate School of

Stephen F. Austin State University

In Partial Fulfillment

Of the Requirements

For the Degree of

Master of Science

Stephen F. Austin State University

December 2018

**Delineation of Karst Potential Using LiDAR and GIS Analyses
Fort Hood Military Installation, Coryell County, Texas**

By

Colby Reece, Bachelor of Science

APPROVED:

Dr. Melinda Faulkner, Thesis Director

Dr. Kevin Stafford, Committee Member

Dr. Wesley Brown, Committee Member

Dr. I-Kuai Hung, Committee Member

Pauline M. Sampson, Ph.D.
Dean of Research and Graduate Studies

ABSTRACT

Traditional karst surveys require extensive field investigations to completely characterize large areas. They are often time-consuming, requiring up to several years to collect and categorize data. Bias is given to areas that are most easily accessible and false negatives are common. The implementation of geographic information systems (GIS) has aided in the aggregation and standardization of karst data; however, these systems have also been used to develop terrain models that allow the user to remotely delineate sinkholes and other surficial features. The Fort Hood Military Installation is a karst landscape that has been altered significantly for use in military training exercises. The ground surface is covered with karst features that are environmentally and structurally sensitive to surrounding activity. These manifest primarily as sinks, pits, and caves, which are typically less than a few meters in diameter or depth. Previous speleological studies in this area have understated the amount and spatial distribution of karst, particularly in western Fort Hood. The following approach uses LiDAR (Light Detection and Ranging) data to provide a more complete karst inventory for the Shell Mountain, Manning Mountain and Royalty Ridge provinces. Data was processed using a digital elevation model (DEM)

derived from LiDAR to automatically fill and extract areas with localized depressions at sub-meter scale. The resulting polygons were processed through a series of filters that isolated depressions outside the influence of non-karst features and with a depth greater than the vertical accuracy of the LiDAR survey. A karst potential map was produced to characterize the remaining depressions into areas of high and low karst density. Potential sinks are distributed across positive relief features in clusters. Their morphology supports a duality of dissolution and collapse origins. Close comparison with manual surveys and field verification points showed that the results were accurate, if not slightly overestimated. These models will be used to aid future investigations and land use planning at Fort Hood.

ACKNOWLEDGEMENTS

I am very grateful to the Fort Hood Natural Resource Management Branch, especially Charles Pekins, for providing insight about Fort Hood and granting access to the installation and GIS data. I would like to thank my fellow geology students: Jacob Meinerts, Jessica Shields, Heather Dailey, Annie Robison, Kaleb Henry, Sarah Zagurski, Matthew Sailor, and my sister, Elaine, for their help during field observations. On that same note, I want to thank my committee members: Dr. Kevin Stafford, Dr. Wesley Brown and Dr. I-Kuai Hung for all their dedication and contributions to this project. I also want to thank the Geology Department at Stephen F. Austin for providing their facilities and vehicle access. I often relied on the love and support of my family, who also gave up their time to help me achieve my goals. Finally, I would like to acknowledge my thesis advisor, Dr. Melinda Faulkner, for her invaluable encouragement and counsel. Thank you for sharing in every breakthrough and every setback along the way.

TABLE OF CONTENTS

ABSTRACT	i
ACKNOWLEDGEMENTS.....	iii
TABLE OF CONTENTS	iv
LIST OF FIGURES	vi
LIST OF TABLES	x
LIST OF EQUATIONS.....	xi
PREFACE.....	xii
DELINEATION OF KARST POTENTIAL USING LIDAR AND GIS ANALYSES	
FORT HOOD MILITARY INSTALLATION, CORYELL COUNTY, TEXAS..... 1	
ABSTRACT	1
INTRODUCTION.....	3
GEOLOGIC SETTING.....	8
KARST FORMATION.....	12
DEPRESSION IDENTIFICATION AND CLASSIFICATION	15
ANALYSIS & DISCUSSION	41
CONCLUSIONS	50

FUTURE WORK.....	53
REFERENCES.....	54
APPENDIX	59
DETAILED METHODOLOGY.....	59
KARST SURVEY.....	60
LIDAR & DEM PROCESSING	61
DEPRESSION IDENTIFICATION	66
DEPRESSION CLASSIFICATION	69
DEPRESSION ANALYSIS	78
VITA	83

LIST OF FIGURES

Figure 1.1: The location and extent of the Fort Hood Military Installation. The central impact range divides Fort Hood into its eastern and western portions. The study area lies in western Fort Hood.....	4
Figure 1.2: The extent of the study area within western Fort Hood. The focus of this survey is on the areas of high elevation, which include: Manning Mountain, Shell Mountain and Royalty Ridge. Points on this map show the existing karst inventory within the study area. All known karst manifest on areas of significant positive relief.....	5
Figure 1.3: Geologic map of the study area, modified from the Bureau of Economic Geology and sourced from the Texas Natural Resources Information System.....	10
Figure 1.4: Digital elevation model created at 0.5 m resolution using a digital terrain model containing elevation point features.....	18
Figure 1.5: Depressions removed using proximity to four main types of non-karst features: (A) ponds were removed by manually identifying their extent using color-infrared imagery; (B) major drainage paths were automatically delineated using a flow accumulation model and 5 m buffer zone; (C) Major roads were mapped using an existing database, CIR imagery and a hill shade raster. A buffer zone of 15 m was used to capture nearby culverts and engineered drainage; (D) minor roads were delineated manually and assigned a buffer zone of 10 m.....	22
Figure 1.6: Major and minor roads delineated using an existing database from the Fort Hood Natural Resource Division and satellite imagery from the Texas Natural Resources Information System.....	24

Figure 1.7: A normalized difference vegetation index colormap representing different land cover types within the study area. Cover types designated as “bare” or “developed” were used for removal. Data sourced from the Texas Natural Resources Information System.....	26
Figure 1.8: Stream networks and ponds delineated using the <i>Flow Accumulation</i> tool and satellite imagery from the Texas Natural Resources Information System.....	28
Figure 1.9: A modified geologic map (from BEG, TNRIS) of the study area showing only the units susceptible to karst. Note that every known karst feature lies within these two units (Reddell et al., 2013).....	29
Figure 1.10: A slope-based elevation model of the study area overlain by the 13,909 filtered depressions found in the classification process. Most features are aggregated at high elevation points where the Edwards Formation outcrops.....	32
Figure 1.11: A plot of length vs width in potential karst features where length is the major axis. The lower trend represents elliptical shape ($L/W = 2$), while the upper trend represents circular shape ($L/W = 1$). This dataset includes 255 points which were randomly generated from depressions with an area greater than 3 m^2	34
Figure 1.12: Histogram showing the distribution of circularity amongst all potential sinks larger than 3 m^2 . In area ($n= 3589$). Most points lie within the circular to elliptical trend with an average ratio of 1.56:1. It is important to note that some depressions exceed the 2:1 threshold, showing sublinear morphology.....	35
Figure 1.13.: A rose diagram showing the frequency of orientation within the dataset. The average of these orientations is 31.5° (NE-SW), which is consistent with regional fracture orientations (Ferrill & Morris, 2008).....	37
Figure 1.14: Point density map of non-interfering depressions in the survey.....	39

Figure 1.15: Area density map showing the magnitude of concentrated features per km ²	40
Figure 1.16: A newly identified collapse sinkhole with an area measuring over 35 m ² . This feature, like many within western Fort hood, shows near-circularity and significant bedrock displacement...	44
Figure 1.17: A previously mapped collapse-cave structure used as an analog in accuracy assessment.....	45
Figure 1.18: False positive depression that appeared in the potential karst survey. This feature is located approximately 1.5 m outside of the road buffer.....	46
Figure 1.19: A comparison between the area density models created from 0.5 m (left) and 1 m (right) resolution DEM's. Though both models share some peaks, the 0.5 m resolution captures many smaller karst manifestations and provides more accurate coverage..	50
Figure 2.1: 0.5 m digital elevation model created to characterize the landscape of Fort Hood.....	64
Figure 2.2: Flow diagram representing the required processes in the creation of DEM from LAS files.....	65
Figure 2.3: Flow diagram representing the sequence of processes required to extract depressions from a 0.5 m DEM into a polygon shapefile.....	68
Figure 2.4: Major and minor roads delineated using an existing database and satellite imagery.....	70
Figure 2.5: A normalized difference vegetation index colormap representing different land cover types within the study area. Cover types designated as "bare" or "developed" were used for removal....	72
Figure 2.6: Stream networks and ponds delineated using the <i>Flow Accumulation</i> tool and satellite imagery respectively.....	75
Figure 2.7: Geologic Map of the study area showing only the units susceptible to karst. Note that every known karst feature lies within these two units.....	76
Figure 2.8: Flow diagram of the filtering processes used to delineate potential sinks and classify them by their spatial attributes.	77

Figure 2.9: Point density map of non-interfering depressions in the survey.....	79
Figure 2.10: Area density map showing the magnitude of concentrated features per km ²	80

LIST OF TABLES

Table 1: Table of the filtering mechanisms and number of features removed during depression classification. Note that the interference count is slightly greater than the total number of depressions due to an overlap in some filters.....	31
Table 2: Confusion matrix containing the depressions surveyed for accuracy in this study.....	43

LIST OF EQUATIONS

Equation 1.1: $S = \sqrt{\frac{A}{n}}$	19
Equation 1.2: $NDVI = \frac{(NIR-Red)}{(NIR+Red)}$	25
Equation 2.1: $S = \sqrt{\frac{A}{n}}$	63
Equation 2.2: $NDVI = \frac{(NIR-Red)}{(NIR+Red)}$	71

PREFACE

Karst development is prevalent in most of the Fort Hood Military Installation. Due in part to its sheer size, previous efforts to characterize and document features have been relatively small-scale. Field mapping is often costly and time-intensive; more importantly, it is not always possible to traverse the rugged terrain within the installation. Previous studies were largely driven by demand, as military personnel or other individuals would happen upon a new cave or sinkhole and report that feature to the Natural Resource Management Branch. The area would then act as a focal point for a new survey, and all karst in the area were entered into the database. While these surveys allow for detailed observations, they are limited in scope and often biased toward high-traffic areas. Remote sensing has become popular in geologic studies because it characterizes larger areas with reasonable accuracy. LiDAR surveys allow geologists and spatial scientists to study the geomorphology of a site without visiting the actual location.

The following research was conducted in cooperation with the Natural Resource Management Branch of Fort Hood to expand upon their existing karst database and design a model to be used in future investigations. This study

characterizes the karst potential of western Fort Hood, an area that has been significantly impacted by military training activities, using a novel LiDAR-based approach.

This thesis has been prepared in accordance with publishing guidelines established by the publication: *Remote Sensing of Environment* and will be submitted by December 15, 2018 for publishing consideration. In addition to this research, an appendix containing detailed methodologies has been included to aid in any future iterations of this study.

Delineation of Karst Potential Using LiDAR and GIS Analyses

Fort Hood Military Installation, Coryell County, Texas

ABSTRACT

Traditional karst surveys require extensive field investigations to completely characterize large areas. They are often time-consuming, requiring up to several years to collect and categorize data. Bias is given to areas that are most easily accessible and false negatives are common. The implementation of geographic information systems (GIS) has aided in the aggregation and standardization of karst data; however, these systems have also been used to develop terrain models that allow the user to remotely delineate sinkholes and other surficial features. The Fort Hood Military Installation is a karst landscape that has been altered significantly for use in military training exercises. The ground surface is covered with karst features that are environmentally and structurally sensitive to surrounding activity. These manifest primarily as sinks, pits, and caves, which are typically less than a few meters in diameter or depth. Previous speleological studies in this area have understated the amount and spatial distribution of karst, particularly in western Fort Hood. The following

approach uses LiDAR (Light Detection and Ranging) data to provide a more complete karst inventory for the Shell Mountain, Manning Mountain and Royalty Ridge provinces. Data was processed using a digital elevation model (DEM) to automatically fill and extract areas with localized depressions at sub-meter scale. The resulting points were processed through a series of filters that isolated depressions outside the influence of non-karst features and with a depth greater than the survey accuracy. A karst potential map was produced to characterize the remaining depressions into areas of high and low karst density. Close comparison with manual surveys and field verification points showed that the results were accurate and reproducible in the study area. Potential sinks are distributed across positive relief features in clusters. Their morphology supports a duality of dissolution and collapse origins. These models will be used to aid future investigations and land use planning at Fort Hood.

INTRODUCTION

The Fort Hood Military Installation is the largest active duty post in the United States. It covers an area over 880 km² in the southeastern portion of Coryell County and the northwestern portion of Bell County, in Central Texas (Figure 1.1; Hammer, 2011). It is bounded by the city of Gatesville in northwest, Killeen and Copperas Cove in the south and southeast, and the Lake Belton reservoir in the east. The acquisitioned area for the military post was privately-owned rural land until the installment of Fort Hood (formerly “Camp Hood”) at the beginning of World War II, in 1942. The original land use was mostly agricultural, and cattle grazing still dominates some publicly leased land (Pugsley, 2001). There are numerous hydrologic and livestock-related improvements that predate the installment of Fort Hood in the area today.

This study covers the Manning Mountain, Shell Mountain and Royalty Ridge provinces in western Fort Hood (Figure 1.2). The area is approximately 110 km², bounded by the western border of installation and the central “live-fire” range. It is significantly altered and highly developed for training exercises involving heavy vehicle maneuvers and simulated combat. Western Fort Hood

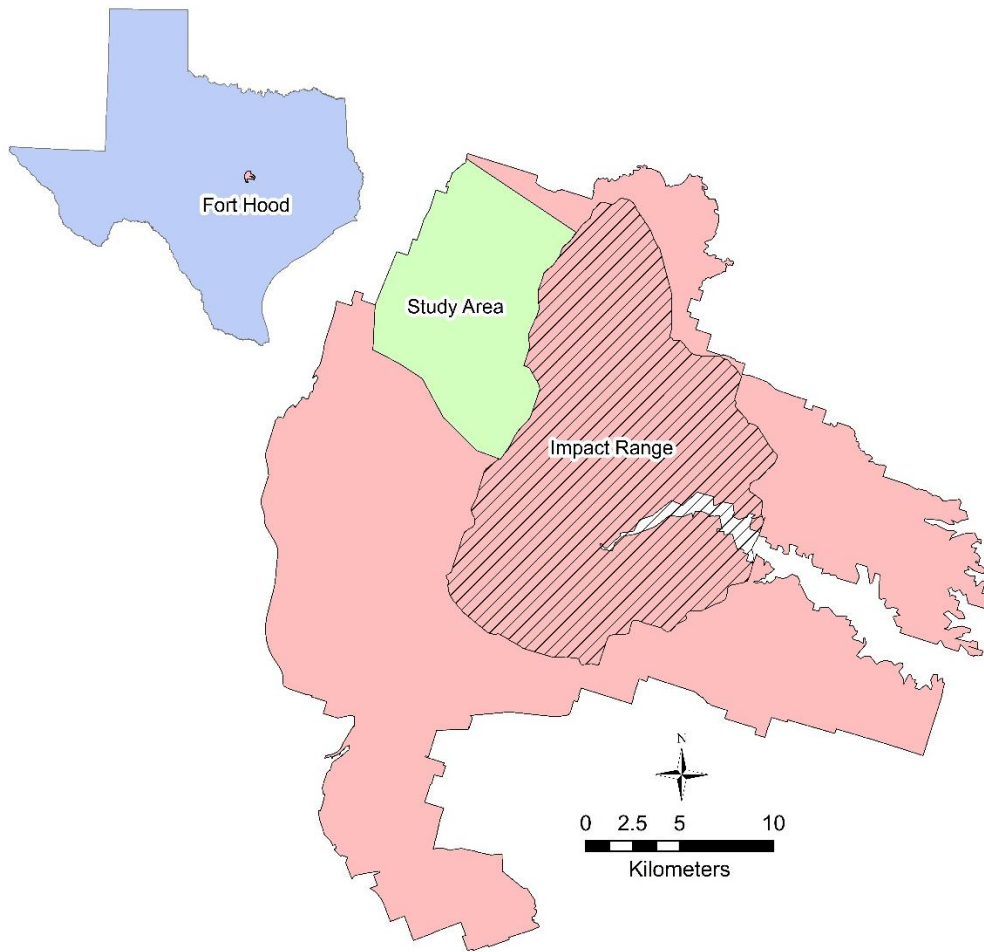


Figure 1.1: The location and extent of the Fort Hood Military Installation. The central impact range divides Fort Hood into its eastern and western portions. The study area lies in western Fort Hood.

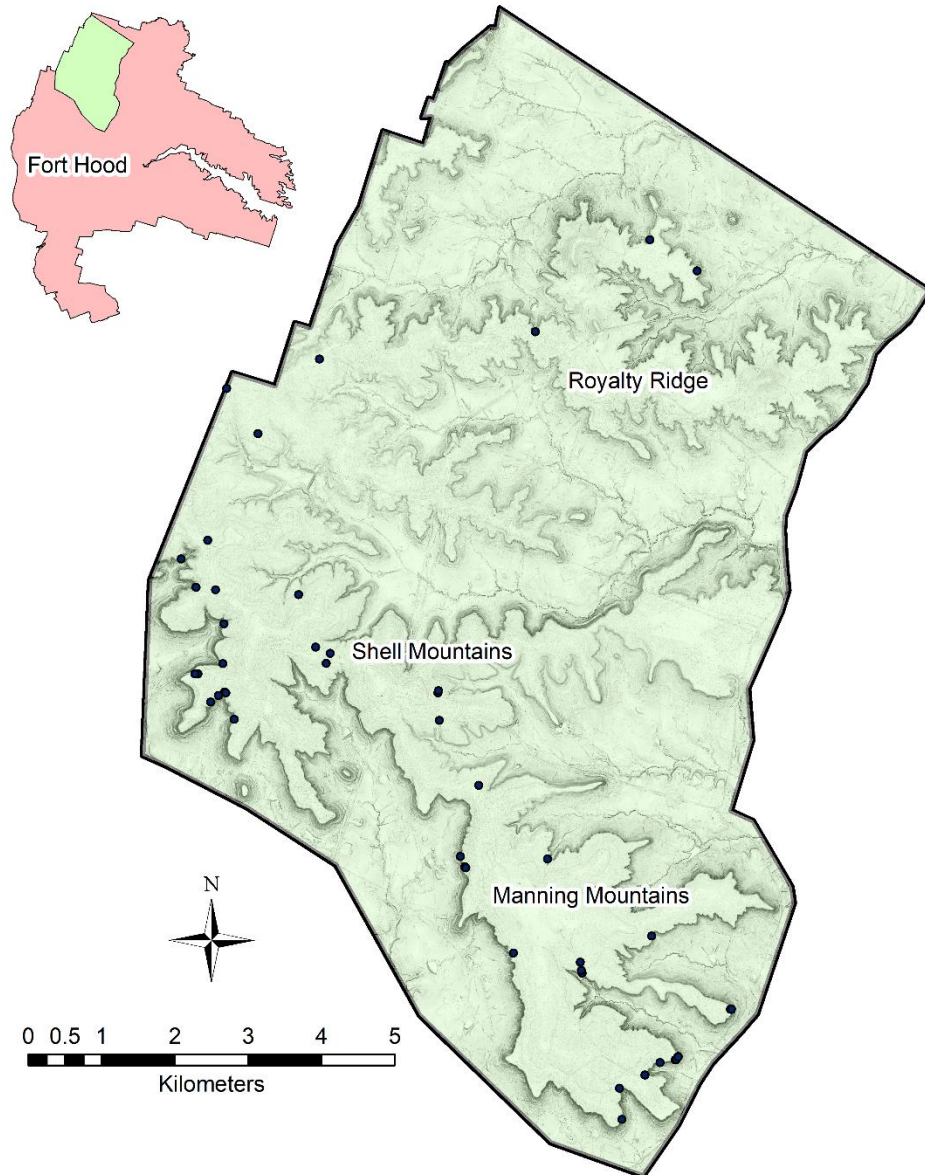


Figure 1.2: The extent of the study area within western Fort Hood. The focus of this survey is on the areas of high elevation, which include: Manning Mountain, Shell Mountain and Royalty Ridge. Points on this map show the existing karst inventory within the study area. All known karst manifest on areas of significant positive relief.

also exhibits numerous sinkholes that act as environmental and structural hazards to military personnel and, to a lesser extent, the greater Fort Hood area.

Sinkholes are closed surficial depressions linked to dissolution of soluble underlying materials. They occur in karst landscapes, where the structure of bedrock beneath the surface degrades and overlying material accumulates in the voids left behind. Sinkholes are prone to collapse as material dissolves, and often act as conduits between surface runoff and groundwater (Faulkner et al., 2016). They are geohazards with potential to cause catastrophic damage and water quality issues in developed areas. Karst inventories have been largely consolidated in the past decades using GIS (Geographic Information Systems) applications and public databases. Previous surveys at Fort Hood were conducted manually using selective ground surveys and subsequent site-verification (Reddell et al., 2011). The results were subjective, targeting areas with heavy traffic and features of significant size. Manual surveys are also time-consuming; a ground survey of the entire installation would take months of consistent work to complete (Wu et al., 2016).

Recent studies have implemented LiDAR (Light Detection and Ranging) to conduct terrain analyses over large areas using dense networks of elevation point data. These modernized surveys can detect surface depressions with greater accuracy and less bias than traditional methods. The purpose of this

study is to delineate potentially hazardous features and update the karst inventory at Fort Hood using GIS applications to increase accuracy and efficiency. Previously successful manual and LiDAR-based surveys in the eastern portion of Fort Hood suggest that LiDAR analysis can adequately characterize the distribution of karst in this region (Bryant, 2012).

GEOLOGIC SETTING

Fort Hood lies within the Lampasas Cut Plain, at the northwestern edge of the Edwards Plateau. The Edwards Plateau extends over much of central Texas and is delineated by the Balcones Fault Zone to the southeast, which separates the plateau from the low-lying Coastal Plain (Bryant, 2012). It is bounded on the east by the Blackland Prairie and to the west by the Chihuahuan Desert (Figure 1.2). The Lampasas Cut Plain is characterized as a transition zone between the Edwards Plateau and the North-Central Plains, and exhibits features that represent this boundary. Topography is generally flat over large expanses, but forms valleys and cliffs near streams (Hayward et al., 1990). The region is dominated by thick Cretaceous carbonates from the Trinity, Fredericksburg and Washita Groups (Amsbury et al., 1984). There are numerous outcrops exposed in the creek beds and along the flanks of smaller plateaus (Adkins & Arick, 1930). The eastern section of Fort Hood is a range of steep plateaus and valleys. Much of the karst manifestations in this region appear as shelter caves and pits, though some sinks have been recorded. Relief is generally high, with steep escarpments separated by sweeping, flat lowlands (Bryant, 2012). The western portion of Fort Hood, by contrast, is broad with extensive plateaus. This area is less susceptible to karst due to the underlying lithology, greater human development and lower relief (Faulkner, 2015).

Surface outcrops in the study area are mostly Lower Cretaceous Trinity and Fredericksburg Group carbonates. These units were deposited approximately 110 mya along the Central Texas Reef Trend on the Comanche Shelf. Fredericksburg Group strata outcrop on positive topographic features, where less sediment has been eroded from the surface. The Trinity Group formations, namely the Glen Rose Formation, outcrops only where overlying strata have been eroded by stream incision in the southeastern portion of the Lampasas Cut Plain (Nelson, 1973). Surface outcrops of the Fredericksburg Group in Fort Hood are generally seen on escarpment faces and hilltops, while the Trinity Group outcrops in stream valleys and other topographic lows (Figure 1.3). Bedding is mostly horizontal or with a gentle dip to the southeast, though many rock surfaces show irregular erosion patterns.

The most important units to this study are the hydrologically sensitive Edwards and Comanche Peak Formations. Most karst manifests at surface outcrops of these units and at their boundaries, which form permeability transitions that promote dissolution. The Comanche Peak Formation is a nodular limestone with interbedded marl sequences. It has a maximum thickness of 21 m in Coryell County and tends to be fossiliferous at the upper boundary (Talbert & Atchley, 2000). Both overlying and underlying contacts are transitional; the Comanche Peak and the Edwards often exhibit complex interfingering at their

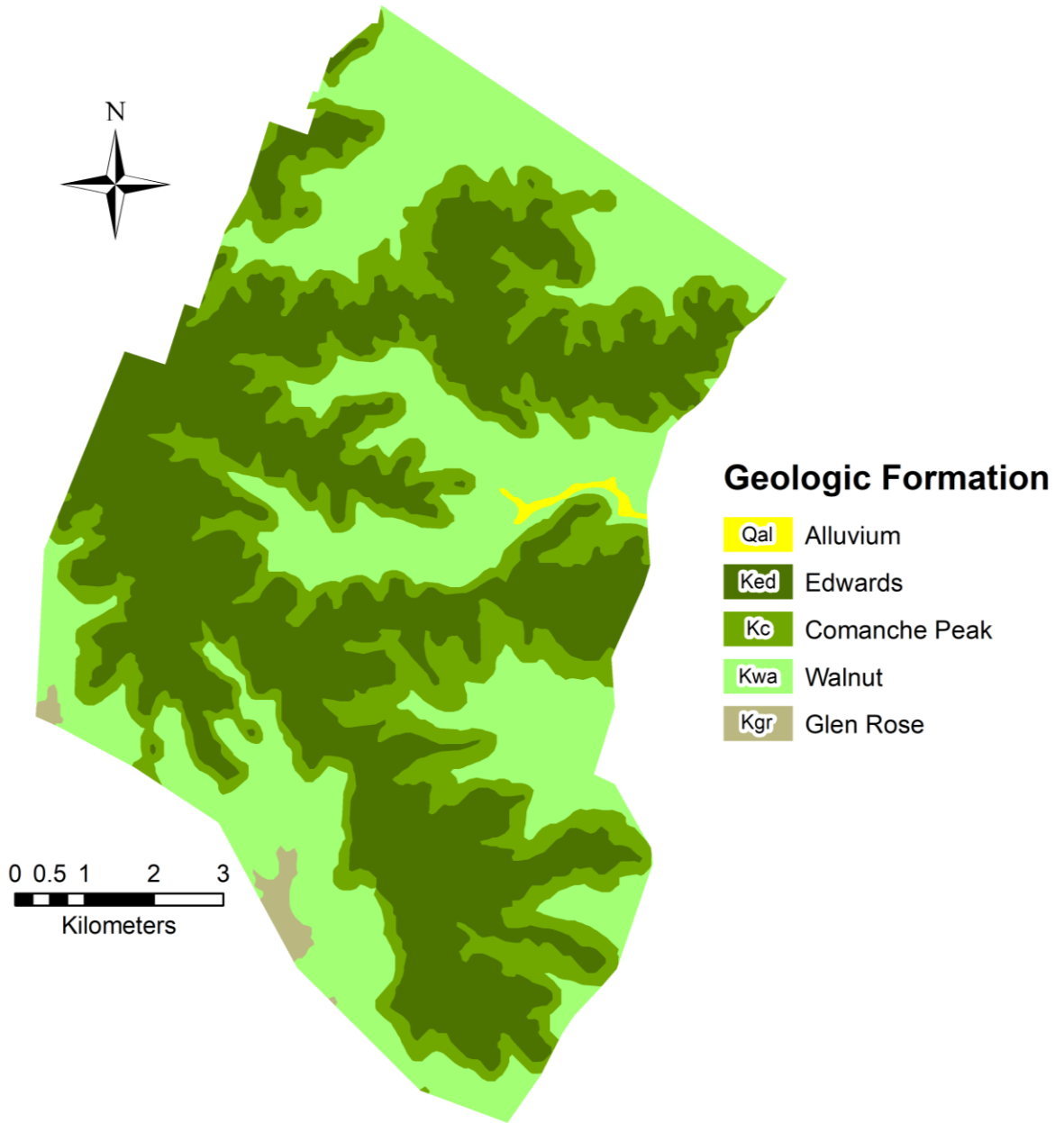


Figure 1.3: Geologic map of the study area, modified from the Bureau of Economic Geology and sourced from the Texas Natural Resources Information System.

boundary (Rose, 1972). The Edwards Formation is a series of massive limestone, dolostones and marls (Fisher & Rodda, 1964). It is typically white in color with abundant rudist bioherms and chert nodules and outcrops at the tops of plateaus and steep escarpments (Stricklin et al., 1971; Scholle et al., 1983). Transmissivity is generally much higher than that of the Comanche Peak Formation, causing a somewhat diagnostic karstic character on erosional surfaces. The thickness of the Edwards Group is greater than 90 m near Austin, Texas; however, the unit thins as it extends north to the study area.

KARST FORMATION

Karst development occurs in three distinct settings: eogenic, hypogenic and epigenic. Eogenic karst occurs in coastal or oceanic areas with young rocks and high primary porosity and permeability. Rocks of this type have usually never left the influences of meteoric waters. Hypogenic karst is associated with fluid circulation at depth, and typically form in semi-confined, soluble rocks (Elliott & Veni, 1994). Epigenic karst occurs in mature, hydrologically unconfined strata that are in direct contact with meteoric waters that recharge from the surface (Klimchouk, 2007). Each of these settings is considered a stage of karst evolution. The most commonly studied and classified type of karst is that of epigenic origin. Recent developments in speleogenetic research have brought an increase to hypogenic karst study and reclassification of epigenic karst.

The Edwards Formation contains numerous types of caves from both epigenic and hypogenic origins. Uplift in the Cretaceous left Edwards Group sediments subaerially exposed, allowing for early development of secondary porosity. A subsequent inundation overlaid the Edwards with fine-grained sediments. Preexisting meteoric water was trapped within the rock for some time, isolated from marine waters. This allowed continued dissolution to take place even when the Edwards was not subaerially exposed. Balcones Fault Zone

deformation in the Paleogene provided another conduit for meteoric water to travel within the Edwards (Anaya & Jones, 2009; Walker, 1979). Low rainfall and low-gradient topography allow water to pool in soil-filled pits that often create sub-hexagonal impressions in the Edwards Formation. Sinkholes are particularly prominent at Fort Hood; the three major types found in this region are dissolution, subsidence and collapse sinkholes. Dissolution sinkholes have little to no overlying sediment, and tend to form as fractures are widened by water at the surface; this type is prominent in the eastern portion of Fort Hood (Bryant, 2012; Faulkner, 2015). Subsidence sinks form where loosely consolidated material (i.e. soil) is piped into voids and fractures in the underlying bedrock; here, suffosion processes dominate, leaving bowl-like depressions as sediment is washed into the subsurface. Finally, collapse sinks are expressed where the structural integrity of the bedrock is compromised by the dissolution beneath a point in the subsurface. Collapse sinks typically intersect existing conduits and may provide cave access as well. They account for the majority of mapped features at Fort Hood; however, this is likely due to the bias given to caves over minor sinkholes (Reddell et al., 2011).

Most known karst on Fort Hood form as shelter caves and collapse features on escarpments and plateaus. Many of the features found in early studies by the Texas Speleological Society (TSS) and the Fort Hood Resource Management Branch were mapped as they were discovered during military

operations or road improvements. Most underground conduits are coupled to the surface in some way, as meteoric water plays a large role in the continued karst development (Reddell et al., 2011). Caves are generally shallow ($> 10\text{m}$), forming in the sides of cliffs and scarps or where sinkholes intersect existing passages. Most caves also form within the Edwards Group; their traverse is usually not extensive ($< 50\text{ m}$), and caves typically end with very small diameter passages that are impassable (Reddell et al., 2011).

DEPRESSION IDENTIFICATION AND CLASSIFICATION

GIS Analyses

Karst inventories have been largely consolidated in the past decades using GIS applications and public databases. Traditional methods for delineating karst involved extensive field time and visual identification from the ground; this commonly results in missed features and subjective distribution. The results are somewhat biased and produced numerous false negatives and positives in sinkhole identification. Manual surveys are also time-consuming, requiring visual study of an entire area and verification of each point (Wu et al., 2016).

Recent studies have shown success using LiDAR (Light Detection and Ranging) surveys to delineate karst features, particularly sinkholes (Wu et al., 2016; Kobal et al., 2014; Doctor & Young, 2013; Faulkner et al., 2013; Bryant, 2012; Angel et al., 2004; Stafford et al., 2002). LiDAR surveys produce high-density point clouds of terrain data, which are used to create highly accurate digital elevation models (DEMs). LiDAR depressions can be classified and categorized using GIS, which automates some processes and greatly increases the accuracy of a survey. Depressions are often classified using the “fill difference” method which detects and fills sinks and then subtracts the original

DEM from the filled raster. Though this process alleviates both time and subjective errors, it also captures all depressions in the survey. Surveys in developed areas are particularly prone to detect non-karst depressions such as culverts, roads and drainage pathways. In addition, fluvial channels and surface runoff create false depressions. Although these studies require extensive buffering and filtering to ensure that only karst depressions are recorded, Geographic Information Systems allow detailed surveys to be completed remotely over large areas with greater accuracy and efficiency.

LiDAR and DEM Processing

LiDAR data was analyzed to automatically detect depressions using Spatial Analyst tools. Raw LiDAR was captured in March 2015 by Quantum Spatial Inc. using airborne surveys. Data was collected over 48 flight lines with 70 control points that covered an 880 km² area over Fort Hood. Data was processed using the DASHMap software package by Optech, Inc. by values for GPS, INS (Internal Navigation System), pitch, roll and heading from the plane's onboard POS (Positioning Orientation System) (Quantum Geospatial, 2015). Statistics were calculated from known ground control points and their respective laser returns, showing a RMSE_(z) of 0.039 m. Vertical accuracy in a LiDAR survey should be 1.96 times greater than RMSE_(z), giving 95% confidence in a

vertical error less than 8 cm over the entire area (Flood, 2004). Horizontal accuracy is largely dependent on the altitude of the scanning unit during the flight; horizontal error was less than 0.01 m with an average point spacing of 0.55 m for this survey (Quantum Spatial, 2015). Classified LAS files were created by Quantum Spatial and later acquired from the Natural Resource Division at Fort Hood. Up to 8 laser returns were recorded at each point, though the majority of points had fewer than 4 returns. The last returns of all points with a “ground” designation were converted to multipoint format to be stored in a geodatabase for use in ESRI’s ArcGIS Desktop 10.5.

LAS files were converted to multipoint features using the *LAS to Multipoint* tool in ArcMap (Figure 1.4). The high density and accuracy of LiDAR data lends itself to storage and memory limitations, so a digital terrain model (DTM) was created to simplify data points. The terrain model was constructed using the *Create New Terrain Wizard* and populated with multipoint files (mass points) containing the elevation data and digitized polylines which represented breaklines in the LiDAR survey. Point spacing used for this new model was 0.5 m; this represents a simplified average of the point spacing in all of the multipoint files and smooths the transition in raster images with the same cell size (ESRI, 2018). The *Terrain to Raster* tool was then used to convert the vector-

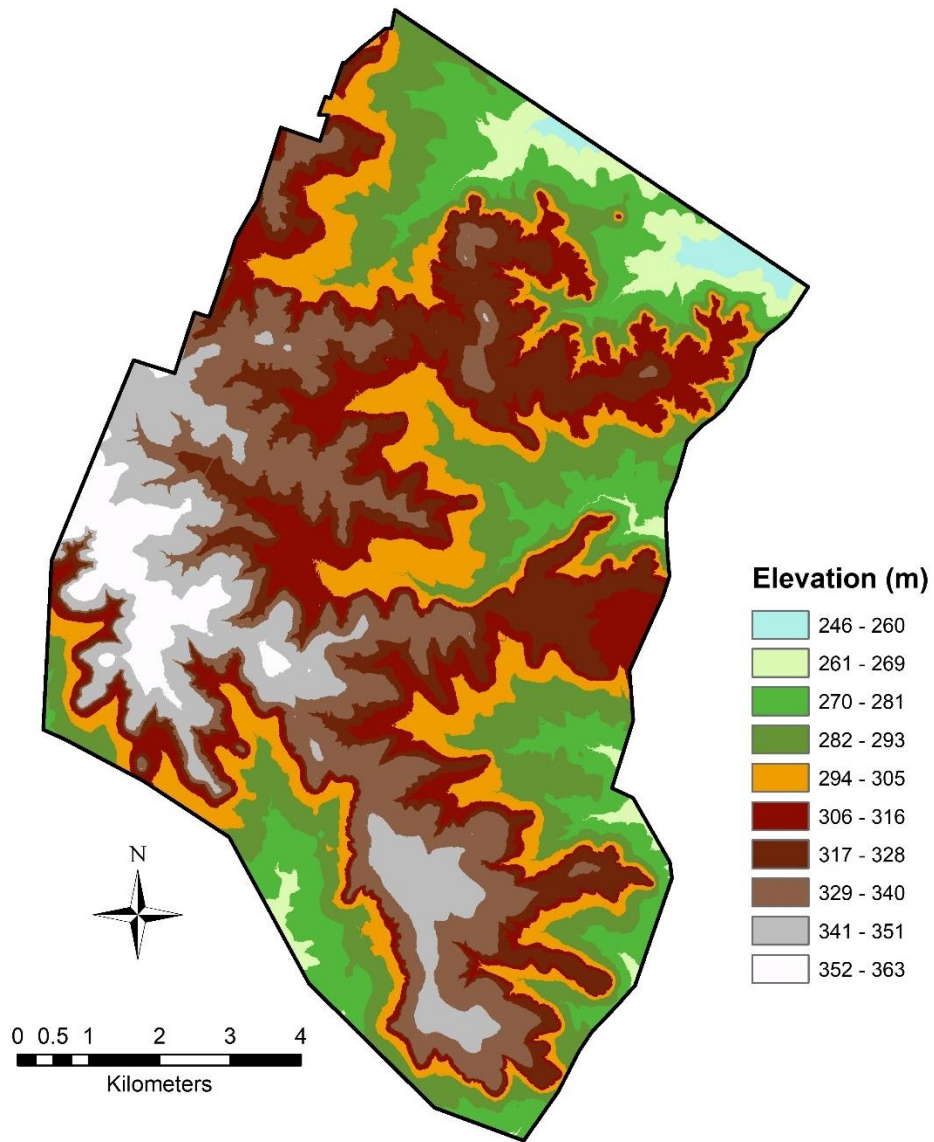


Figure 1.4: Digital elevation model created at 0.5 m resolution using a digital terrain model containing elevation point features.

based DTM into a format that could handle cell-based calculations. The natural neighbor method was chosen for interpolation because it creates a smoother and more accurate model than similar methods without compromising small undulations at the surface (ESRI, 2018). Cell size (i.e. resolution) was determined using:

$$S = \sqrt{\frac{A}{n}} \text{ (Equation 1.1)}$$

Where S is the grid size, n is the total number of data points and A is the area of the DEM (Hu, 2003). This means that grid size should approximate the point spacing of the original survey. It has been determined in previous studies that 1 m resolution is ideal to adequately extract discrete depressions without introducing significant error; however, these studies were conducted without access to data with sub-meter resolution. The resulting 0.5 m DEM (digital elevation model) allowed detailed spatial analyses of the relationship between cells, specifically using the *Hydrology* extension under the *Spatial Analyst* toolbox.

Depression Identification

Depressions can be detected from digital elevation models in several ways. Early studies used models that measured relative position to find negative

anomalies by creating a TPI (topographic position index) raster or calculating slope. These models lack spatial context, however, and require extensive subjective filtering by the user. They also work best in raster models with very low elevation tolerances (i.e. low relief), and thus would not be suited to characterize an area with over 100 m of relief (Angel et al., 2004; Wang & Liu, 2006). Sinkholes are best treated as hydrologic anomalies rather than topographic anomalies, where connectivity to other areas of flow accumulation is taken into consideration. The *fill-difference method* outlined in this section uses an inclusive tool that was originally designed to reduce surface complexity to extract features with a pour point. Pour point defines the height of the watershed above an isolated depression and is often referred to as the spill elevation (Wang & Liu, 2006).

Depressions were identified within this model using the *Fill* tool under the *Hydrology* extension in ArcMap. The *Fill* tool uses an iterative process that determines flow direction and finds areas where an outward direction does not exist. It then fills that cell to its pour point to correct the flow direction and repeats this process until there are no “sinks” left in the raster (ESRI, 2018). This tool was originally intended to remove anomalies and smooth data for flow calculations; however, it has proven useful in identifying depressions as well. *Fill* is a scripted combination of several other processes that identify the pour point of cells and raise the elevation (z) field to that value in a new raster.

After depressions were filled to their pour point, they were extracted using *Raster Calculator* to subtract values in the original DEM from those in the newly-filled DEM. The fill-difference (or “minus”) raster showed only values for the calculated depth of depressions as all other values were reduced to zero. Using the *Set Null* tool, these zero values were removed from the raster to isolate depressions from the background. The depression raster was converted to a polygon shapefile to use feature class based filtering tools. *Raster to Polygon* was used to convert the image from cell to vector format and measure the spatial attributes of each depression. Depression polygons were then redefined by dissolving boundaries between cells and simplifying the shape of discrete features. Since the *Fill* tool shows only the innermost spill point, a 0.5 m buffer was applied to each feature to better represent overall size and reduce resolution oversight. Depressions were then filtered based upon their spatial attributes and proximity to specific features. Ponds, streams, roads and other developed areas may contain depressions that are not related to karst (Figure 1.5).

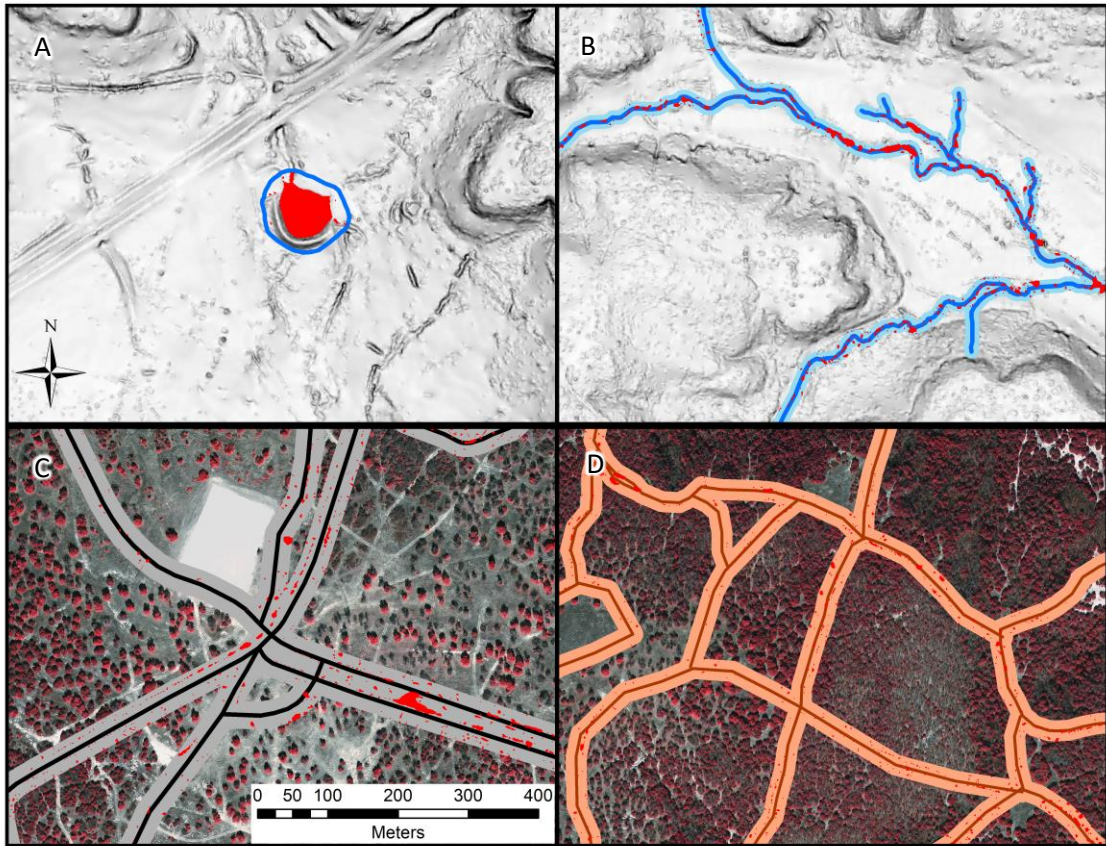


Figure 1.5: Depressions removed using proximity to four main types of non-karst features: (A) ponds were removed by manually identifying their extent using color-infrared imagery; (B) major drainage paths were automatically delineated using a flow accumulation model and 5 m buffer zone; (C) Major roads were mapped using an existing database, CIR imagery and a hill shade raster. A buffer zone of 15 m was used to capture nearby culverts and engineered drainage; (D) minor roads were delineated manually and assigned a buffer zone of 10 m.

Depression Classification

The method described above identified 100,180 depressions within the extent of the DEM. Many of these features are not karst-derived, but rather controlled by anthropogenic and geomorphological processes which form false positives that may be mistaken for sinkholes. Depressions must be filtered and classified by their spatial relationships with other existing features such as roads, streams and other water bodies. Furthermore, the underlying geology should be susceptible to dissolution and localized topographic relief (cliffs, incised valleys, etc.) should not exist nearby. Most of the depressions found in this study had depths less than 1 m; however, potential sinkholes with a depth that did not exceed the vertical accuracy of the LiDAR survey (0.077 m) could not be considered due to the lack of confidence in identification.

Depressions in proximity to roads and other developed areas were removed first, using manually delineated features and land cover types. Major roads transect the entire study area, and are usually accompanied by engineered drainage and internal depressions. Aerial imagery (from the LiDAR survey) was used to digitize the centerline of all major roads; most were constructed with two lanes and divided at the center (Figure 1.6). A buffer zone of 15 m was then applied to the road polylines to incorporate nearby ditches and culverts. Minor

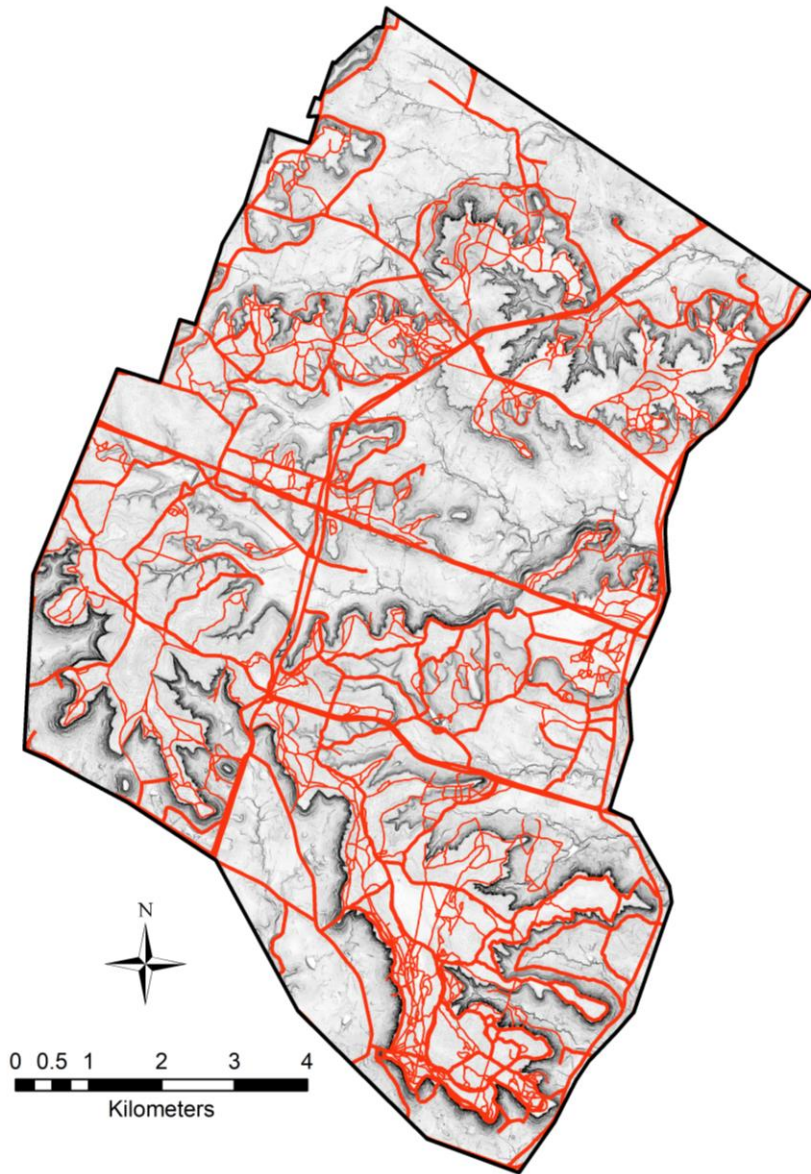


Figure 1.6: Major and minor roads delineated using an existing database from the Fort Hood Natural Resource Division and aerial imagery from the LiDAR survey data package.

roads consist of trails, tank roads and smaller byways connecting the major roads. Their width is almost never greater than 5 m and the associated drainage areas are less pronounced. These roads were digitized and given a 10 m buffer from the centerline to incorporate only the immediate trail areas. Training sites, unpaved lots and other developed areas were delineated by measuring the spectral intensity of the land surface. Intensity is a measure of the amount of light that is reflected from an object at the surface. Light is represented by a spectrum of different wavelengths and categorized by ranges within that spectrum. Intensity is often collected in several bands representing each different wavelength and recorded for each cell with a value between 0 and 255. NDVI (Normalized Difference Vegetation Index) is commonly used to distinguish land cover classes and is calculated by:

$$NDVI = \frac{(NIR-Red)}{(NIR+Red)} \text{ (Equation 1.2)}$$

where “NIR” and “Red” represent the intensity of their respective wavelength within each cell (Pettorelli et al., 2005). The *NDVI* function under *Image Analysis* was used to produce a land cover map showing the different landscape types at the surface (Figure 1.7). Areas designated as “developed” or “bare-ground” were used to filter and remove depressions.

Streams, rivers and ponds were delineated to remove natural depressions that are not related to karst processes. Water bodies naturally incise the

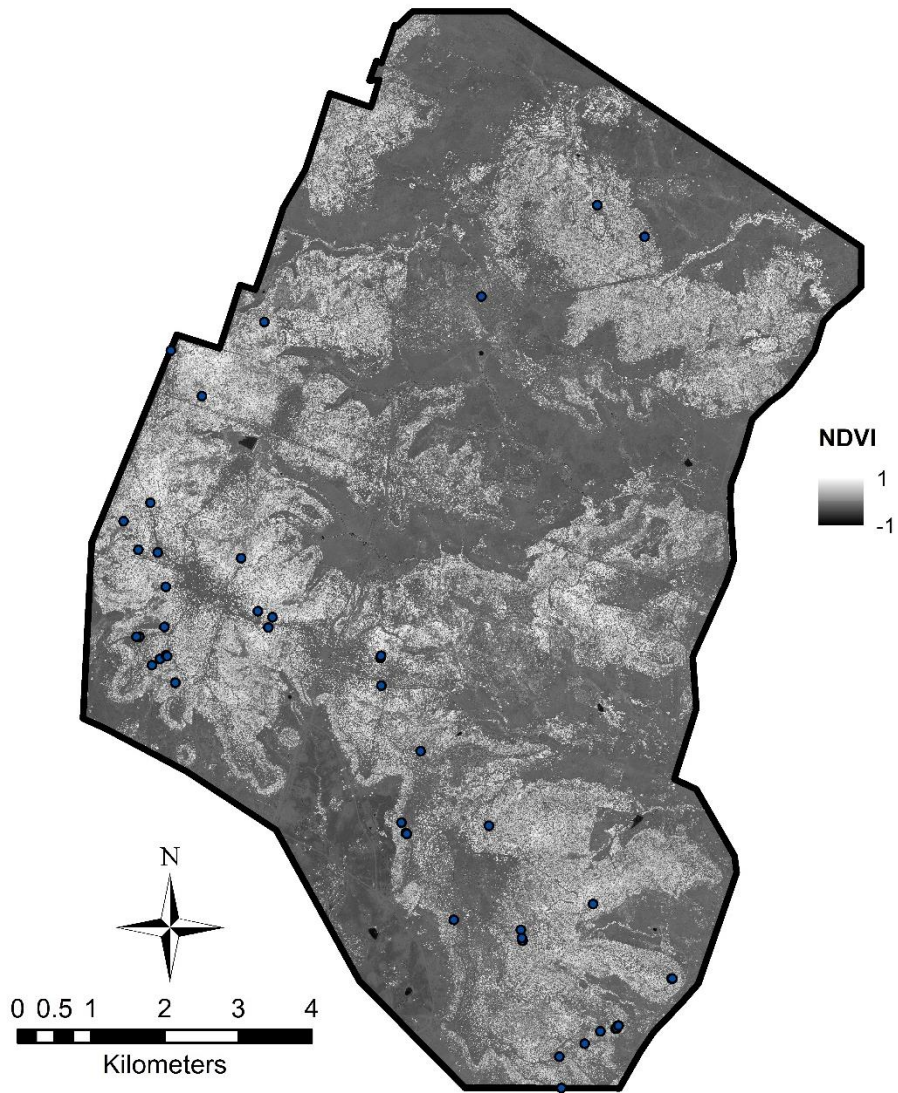


Figure 1.7: A normalized difference vegetation index colormap representing different land cover types within the study area. Cover types designated as “bare” or “developed” were used for removal. Data sourced from the Texas Natural Resources Information System.

landscape, forming anomalous lows in streambeds that can appear as isolated sinks. Ponds were manually digitized and buffered to include 20 m of the immediately surrounding area. Streams were delineated using a flow accumulation raster. Flow accumulation measures the accumulated weight of all cells flowing into a cell of lower elevation. Areas of the high concentrated flow can be used to map streams and form a network of interconnected high-accumulation cells (Figure 1.8; ESRI, 2018). Streams were given a 5 m buffer from their centerline to include only the immediate drainage path.

Depressions were then classified by their underlying lithology using a modified geologic map from the Texas Natural Resources Information System. Any potential sinkholes in the area that do not overlie the hydrologically sensitive Edwards or Comanche Peak formations were not considered as karst manifestations. The geologic map of the Shell Mountain Province was acquired and modified from the Bureau of Economic Geology and applied as a filter to remove depressions overlying the Walnut formation (Figure 1.9). The depth of each depression was compared to the vertical accuracy of the LiDAR survey, which was calculated as 0.077 m. Any depressions whose depth did not exceed the vertical accuracy had to be dismissed from further evaluation. Though some shallow sinkholes were likely removed from the study during this step, those depressions could not be accurately resolved using this model. The resulting polygons represented depressions that did not interfere with any filter.

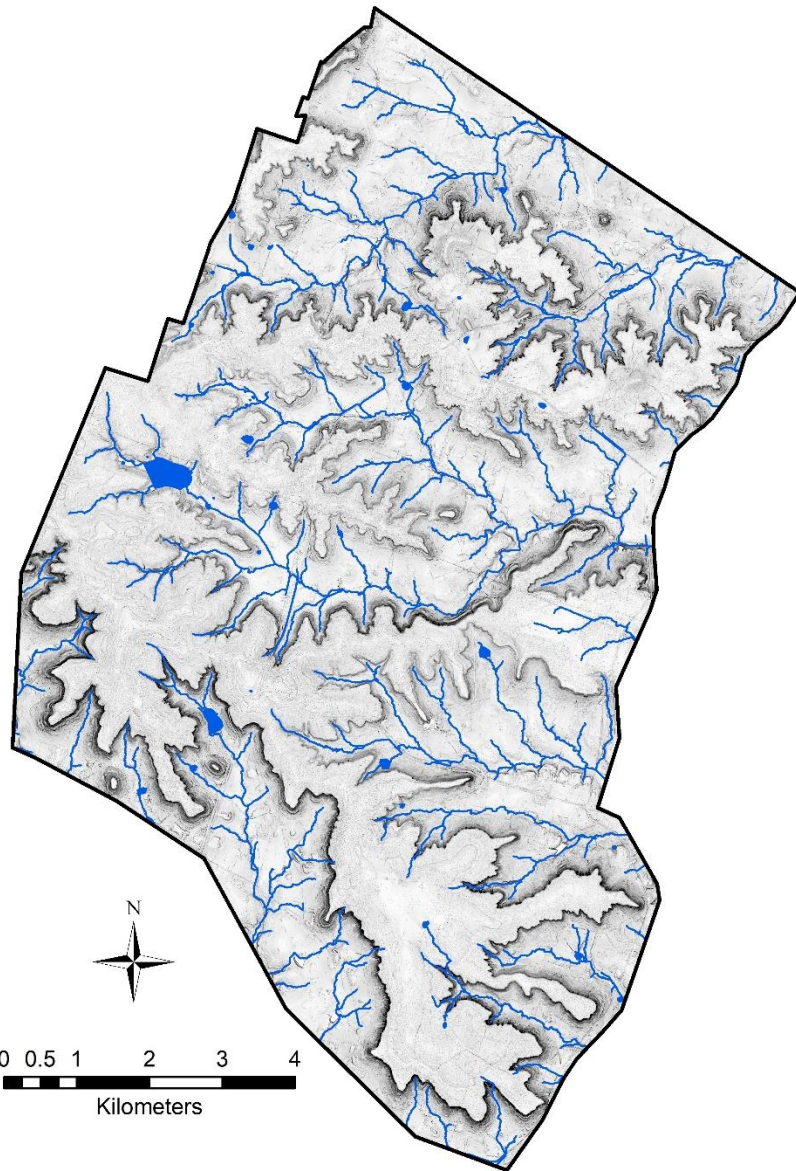


Figure 1.8: Stream networks and ponds delineated using the *Flow Accumulation* tool and aerial imagery from the LiDAR survey data package.

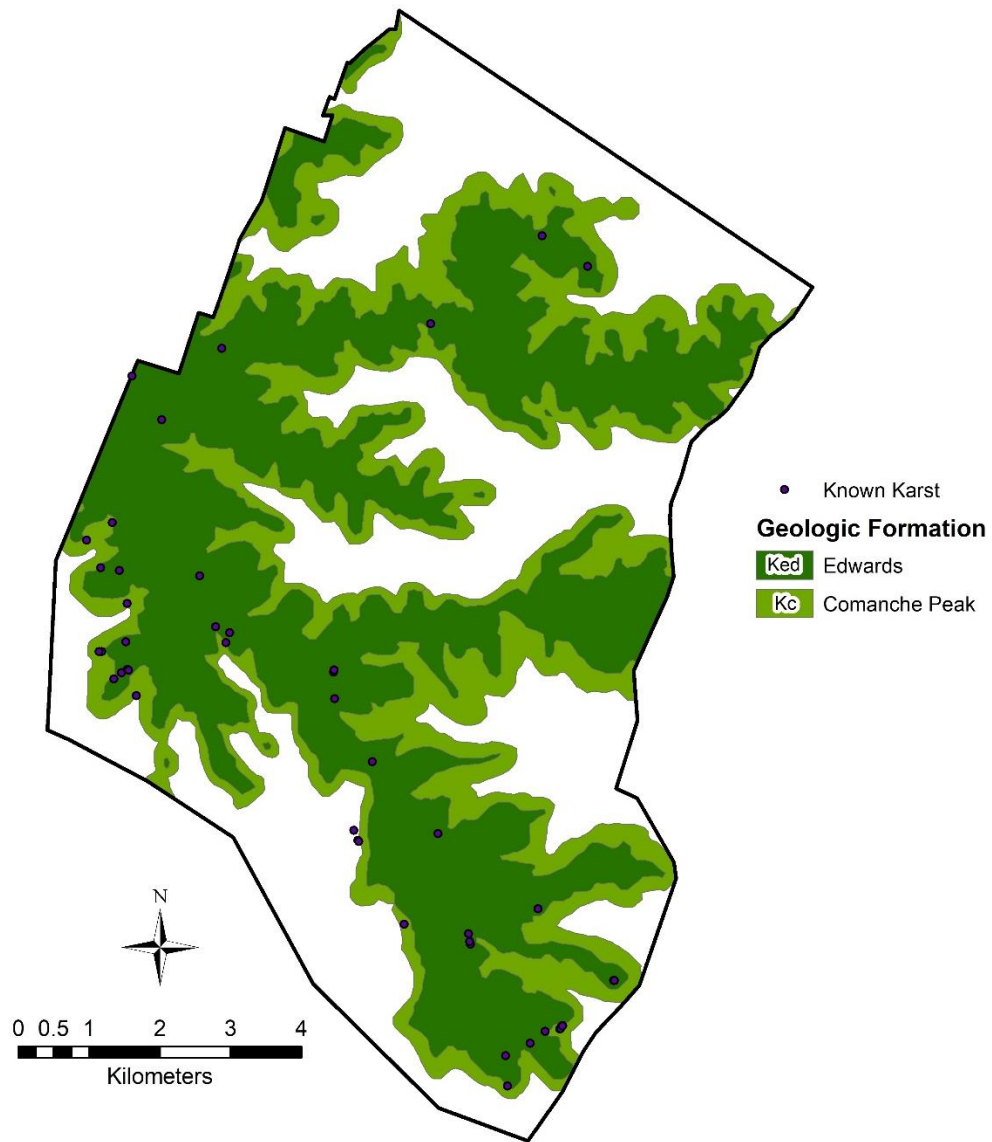


Figure 1.9: A modified geologic map (from BEG, TNRIS) of the study area showing only the units susceptible to karst. Note that almost every known karst feature lies within the Edwards Formation or its boundary with the Comanche Peak Formation (Reddell et al., 2013).

The total number of features that interfered with each individual filter is shown in Table 1; this represents the number of interfering features from the entire depression inventory regardless of overlap. The remaining 13,909 sinks were simplified and smoothed to best represent their spatial extent rather than the shape and size of their pour point. These polygons represent the extent and distribution of the most probable karst depressions (Figure 1.10).

Sinkhole Morphology and Lineament

The morphology of each feature was analyzed by its length to width ratio to determine circularity; previous surveys indicate that most mapped features in this part of Fort Hood are partially collapsed and should exhibit near circular patterns (Reddell et al., 2011). Non-interfering sinkholes were classified by their circularity to characterize the relative stage of development through degree of collapse. This provided a way to gather statistics on the shapes of depressions and, to a lesser extent, describe the accuracy of delineated sinks. The ratio of length (major axis) to width (minor axis) should be 1:1 in a perfect circle and should not exceed 2:1 in sinkholes, which tend to be less elliptical than other depressions (Gutierrez et al., 2006; Ford and Williams, 2007).

Table 1: Table of the filtering mechanisms and number of features removed during depression classification. Note that the interference count is slightly greater than the total number of depressions due to an overlap in some filters.

Interference Type	Filter	Interference Count
Major Roads	15 m	6,859
Minor Roads	10 m	4,983
Streams	5 m	12,969
Water Bodies	20 m	287
Geology	Lithology Shapefile	42,378
Land Cover	NDVI	6,627
Depth	< 0.077 m	46,568

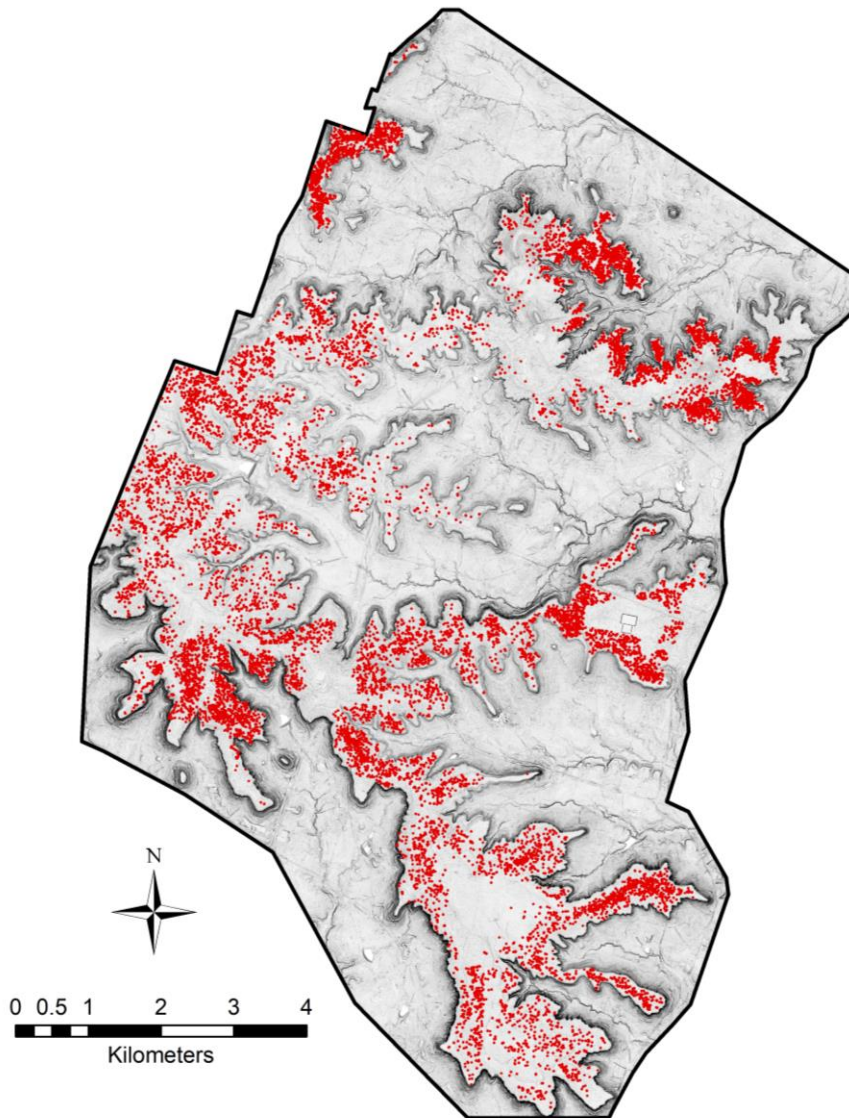


Figure 1.10: A shaded relief map of the study area overlain by the 13,909 filtered depressions found in the classification process. Most features are aggregated at high elevation points where the Edwards Formation outcrops.

Dimensions were calculated for each potential sinkhole using the *Minimum Bounding Geometry* tool to create rectangles with more easily measurable dimensions. Since many features are too small to accurately represent at 0.5 m resolution, only depressions with an area greater than 3 m² were considered. The values were put into a table in *Microsoft Excel* and graphed using length in the x-axis and width in the y-axis (Figure 1.11). Two lines were created with a slope of 1 and 2 to represent circular and elliptical shapes respectively. A histogram was also created for the dataset, showing an average circularity ratio of 1.56:1 (Figure 1.12). This revealed a bimodal distribution with points clustered near both ends of the spectrum. Most potential sinks between a 1:1 and 2:1 ratio trend toward a more circular habit than elliptical (suggesting collapse or subsidence origins); however, the large clusters of sub-linear depressions suggest that there could be a fracture-controlled component influencing sinkhole manifestations as well; these depressions could also be incised and overprinted by other processes. The asymmetry of depressions found in this study was compared to these standards and showed minimal deviation from circular or elliptical shape in most instances. Variations from circularity in this case were likely dependent on the stage of formation in the depression. Solutional widening of fractures and the gradual collapse of horizontal conduits also create more elongate features in some instances (Kobal et al., 2015).

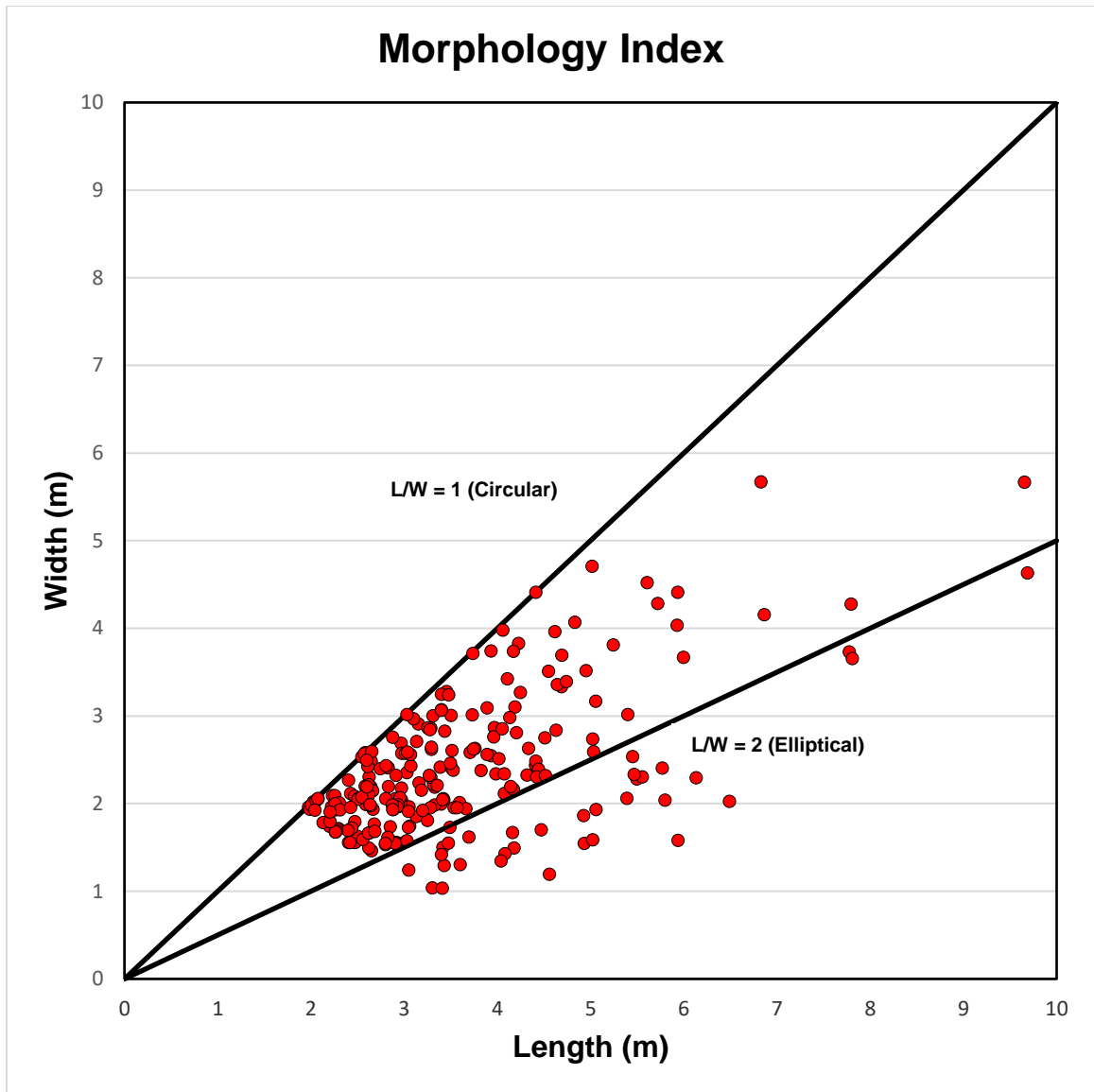


Figure 1.11: A plot of length vs width in potential karst features where length is the major axis. The lower trend represents elliptical shape ($L/W = 2$), while the upper trend represents circular shape ($L/W = 1$). This dataset includes 255 points which were randomly generated from depressions with an area greater than 3 m.

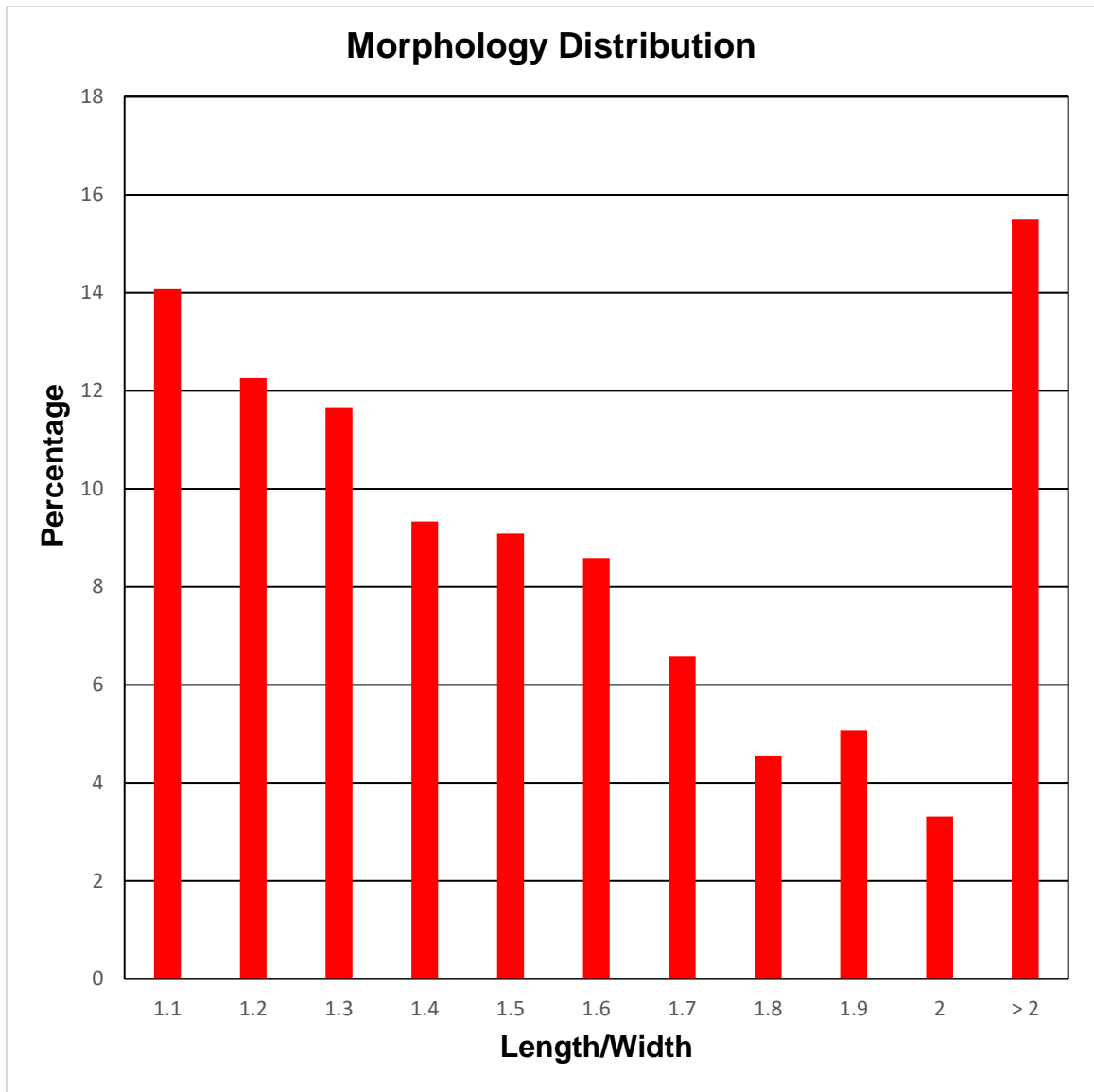


Figure 1.12: Histogram showing the distribution of circularity amongst all potential sinks larger than 3 m² in area (n= 3589). Most points lie within the circular to elliptical trend with an average ratio of 1.56:1. It is important to note that some depressions exceed the 2:1 threshold, showing sublinear morphology.

Minimum Bounding Geometry also recorded the orientation of the long axis in each depression. These orientations were classified by the azimuthal direction with values ranging from 0-180 degrees. The lineament of each depression was exported to a rose diagram to display trends found within the dataset (Figure 1.13). The average of these values is approximately 31 degrees, and many of the potential sinks exhibited a NE-SW trend. This is consistent with fractures and joint associated with Balcones deformation (Ferrill & Morris, 2008). Previous lineament analyses in eastern Fort Hood revealed a similar trend in the linear directions of both joints and sinkholes; the study suggested that the trend exists due to the relationship between dissolution and fracture porosity (Faulkner, 2016).

Karst Potential

While an inventory of depression polygons is useful in characterizing individual features, the inherent limitations of LiDAR surveys create at least some false positives and negatives. A more useful way to interpret the large-scale distribution of sinks is by creating a karst potential model. Karst potential is a generalized concentration of karst-related depressions in an area. The *Kernel Density* tool was used to determine which areas contained the most significant karst manifestations. Polygons were converted to individual points and used to produce two raster models: the first measured the number of features in a

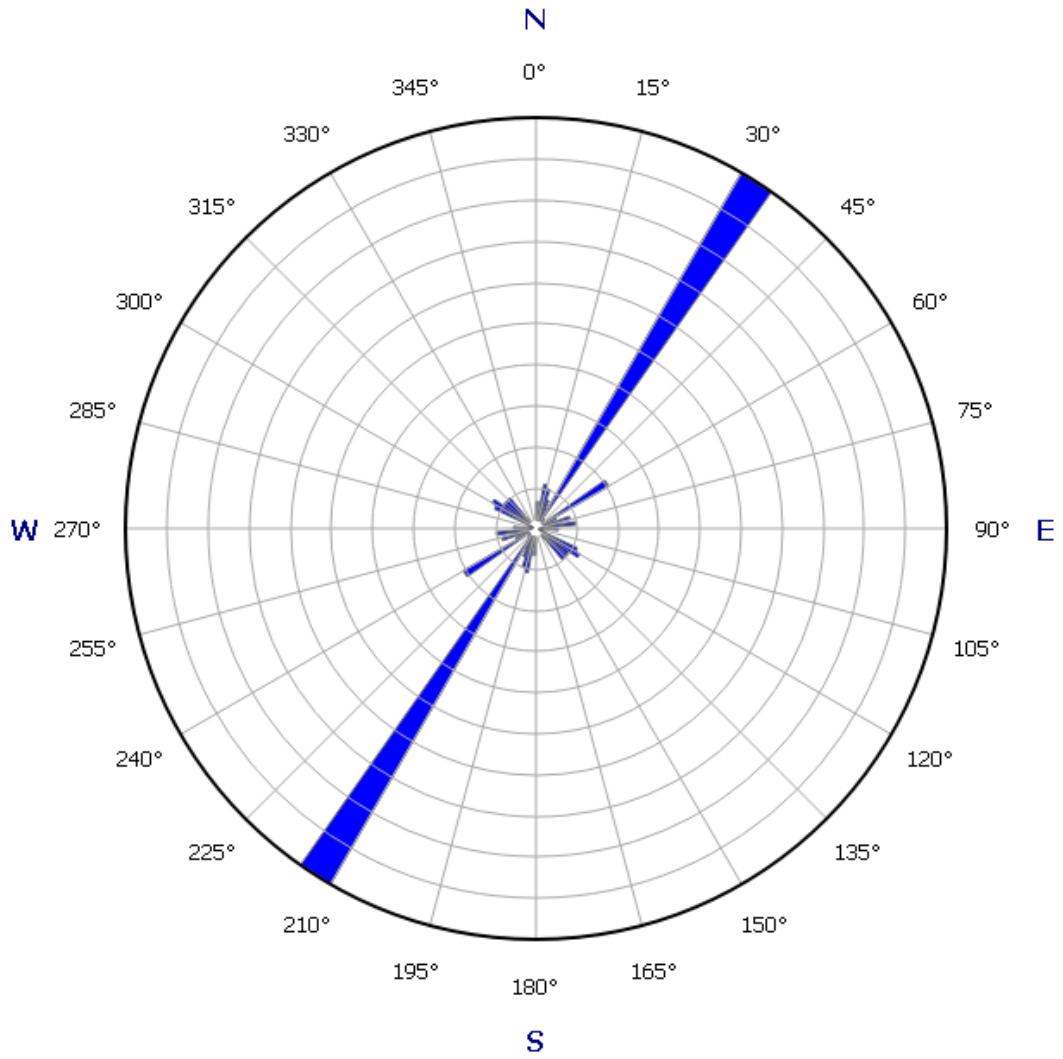


Figure 1.13.: A rose diagram showing the frequency of orientation within the dataset. The average of these orientations is 31.5° (NE-SW), which is consistent with regional fracture orientations (Ferrill & Morris, 2008).

neighborhood of 1 km², while the second measured the surface area of features using the same neighborhood of 1 km².

The point density model showed the greatest concentrations at areas of high elevation, particularly at the western border of Fort Hood where the Shell Mountain Plateau peaks in elevation (Figure 1.14). An additional area-density model was created to better represent the magnitude of the sinks in an area (Figure 1.15). Point density takes an unbiased account of the occurrences in an area, which can mislead interpretations when most features are closer in size to karren (in the form of pits or potholes) than sinkholes. The distribution of sinks in both models supports the initial observation that karst are relatively clustered in pockets of soluble rock within the study area. More importantly, the density of karst in this survey does not match the density of previously mapped features; this exemplifies the disconnection between what has been surveyed and what likely exists at the surface (Reddell et al., 2013).

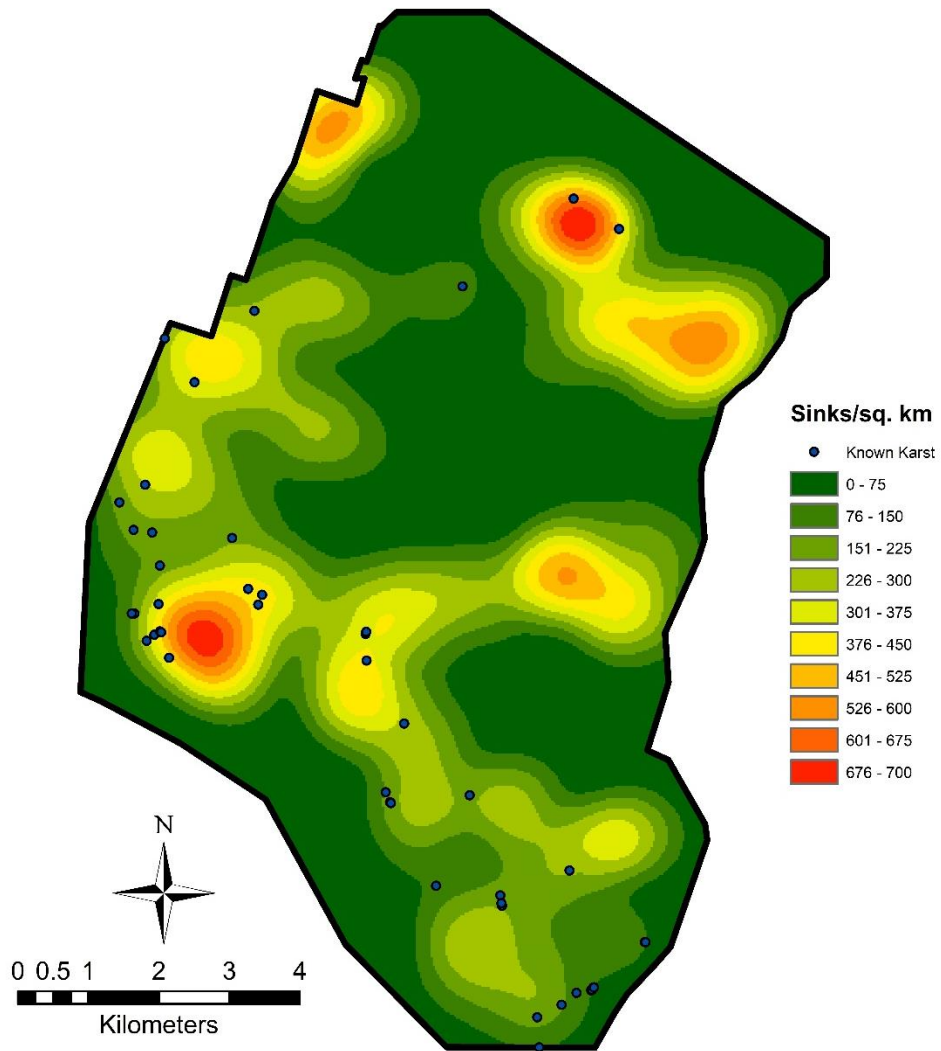


Figure 1.14: Point density map of non-interfering depressions in the survey.

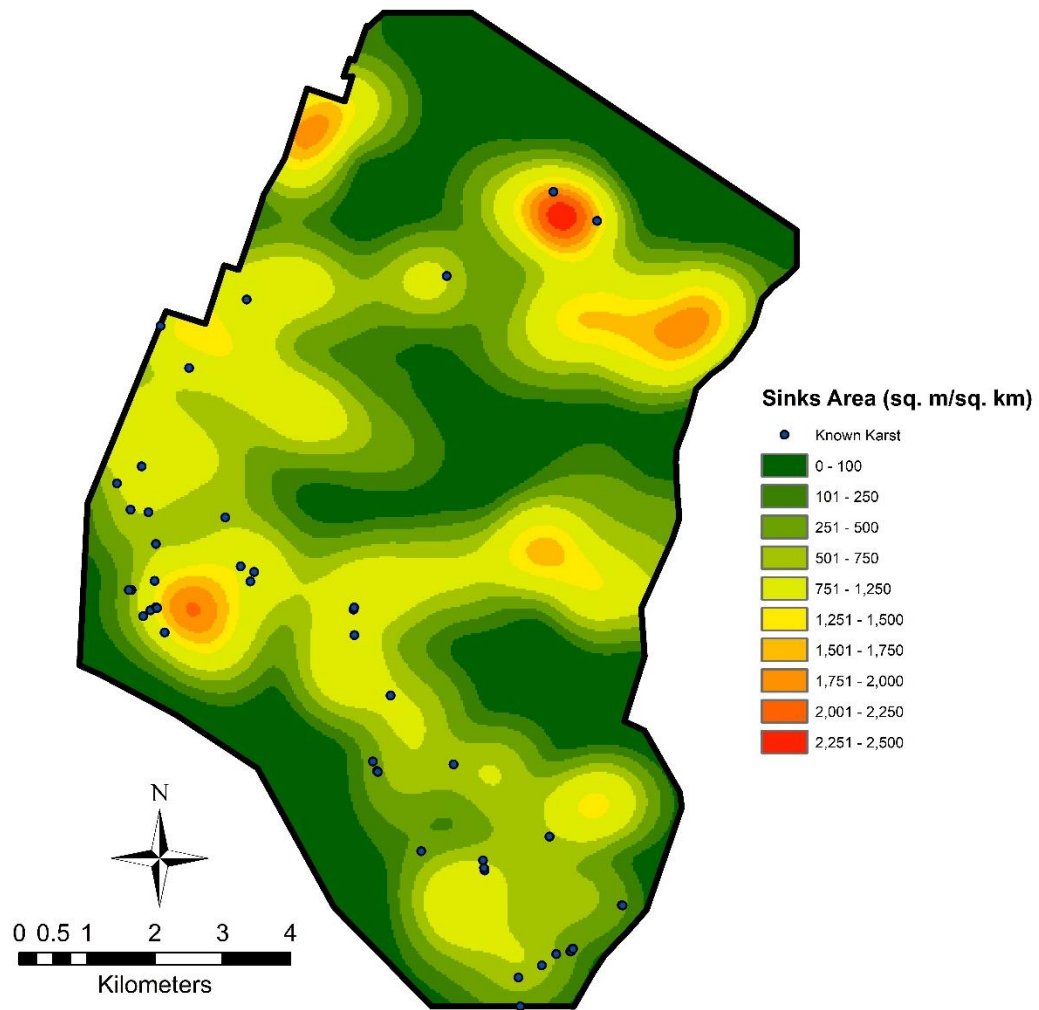


Figure 1.15: Area density map showing the magnitude of concentrated features per km².

ANALYSIS & DISCUSSION

Accuracy Assessment

Accuracy was measured by selecting and verifying random features that were delineated in this study. Initial investigations targeted areas containing the most distinct artificial (non-karst) and known karst features, comparing the shape, size and location of depressions on the ground and in the LiDAR survey. Positive correlations supported the accuracy of other potential sink locations and provided a basis for further field verification. Sinkholes were measured by the length of their major axis and maximum depth, then compared with the entire potential sink inventory.

The *Create Random Points* tool was used to generate a list of 50 potential karst features for confirmation. An additional 50 points were generated from the removed (i.e. filtered) depressions to assess the abundance of false negatives derived from the survey and further increase filter efficiency. Field checks were conducted at each location to verify the model classification and record measurements of each feature. When combined with initial investigations (46 sinkholes) and previously known karst features (29 sinkholes and surface caves), a total of 175 individual depressions were considered in this accuracy

assessment. The results were categorized by their predicted and true conditions and entered in a confusion matrix (Table 2). 115 depressions were recognized by the model as potential karst, while the other 60 were not detected or removed during filtering. Of those 115 predicted positive depressions, 101 were verified as corresponding to a real sink; this gave a commission error of 12.2%. The predicted negative depressions returned 4 false negatives, giving an omission error of 6.7%. The model, therefore, returned an overall true accuracy of 89.7% with a tendency to overestimate the number of depressions in a given area. This is due in part to the difficulty in filtering out small interferences such as off-road trails with significant vegetative cover. The omission error is indicative of a high degree of success in the areas that were filtered. Only a handful of the removed depressions were too aggressively filtered (Stehman, 1997).

Figures 1.16, 1.17 and 1.18 show newly identified, previously known and falsely identified karst depressions recorded in this survey. The resolution of both the survey and satellite imagery is likely to have caused similar false positives in the study area; however, the degree of accuracy provides confidence in the characterization of other features in the study area. False positives near trails were used to update the minor road buffer extent.

Table 2: Confusion matrix containing the depressions surveyed for accuracy in this study.

<i>Total Depressions: 175</i>	<i>True Positives</i>	<i>True Negatives</i>	
<i>Predicted Positives</i>	101	14	Commission Error: 12.2%
<i>Predicted Negatives</i>	4	56	Omission Error: 6.7%
			<i>Overall Accuracy: 89.7%</i>



Figure 1.16: A newly identified collapse sinkhole with an area measuring over 35 m². This feature, like many within western Fort hood, shows near-circularity and significant bedrock displacement.

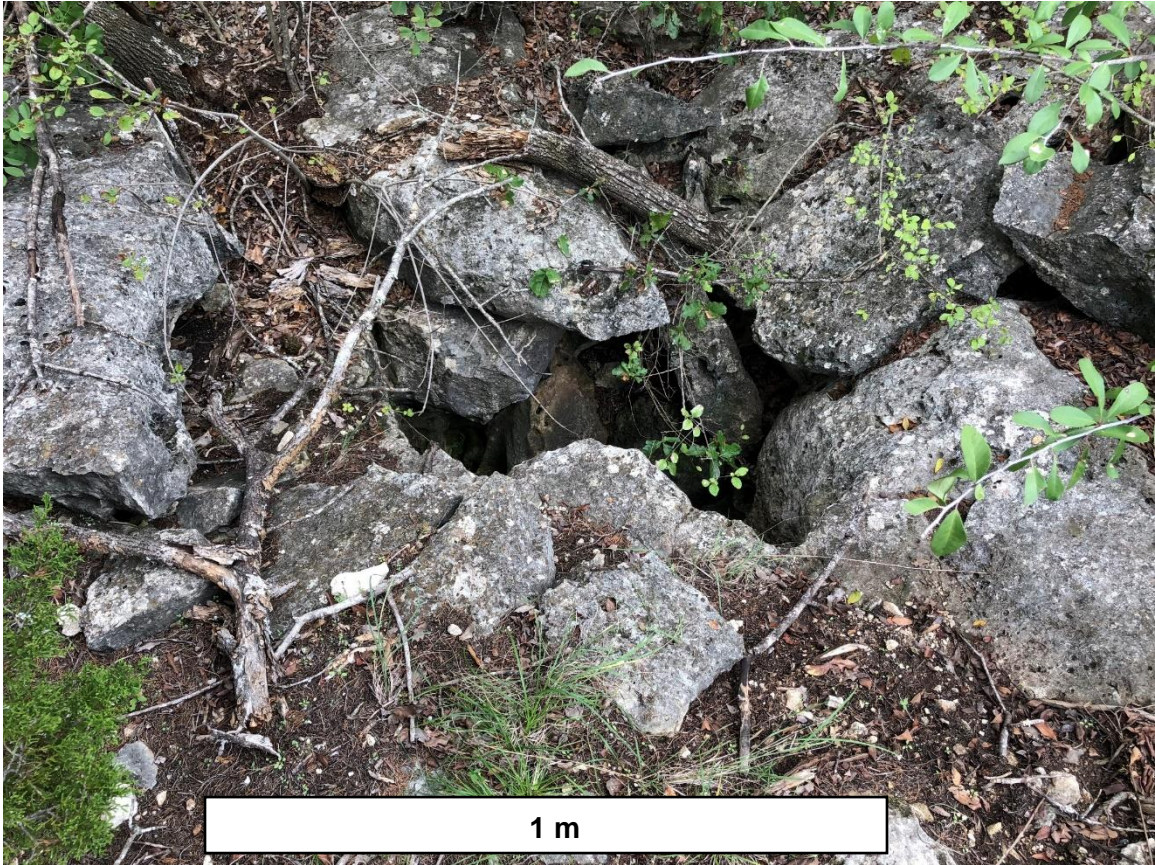


Figure 1.17: A previously mapped collapse-cave structure used as an analog in accuracy assessment.



Figure 1.18: False positive depression that appeared in the potential karst survey. This feature is located approximately 1.5 m outside of the road buffer.

Model Limitations

The fill-difference method used in this study detected over 100,000 individual depressions; however, most were subsequently removed through extensive filtering. Only 13,909 (~10%) of these depressions were interpreted as sinkholes of adequate depth and location. High-volume datasets often produce convoluted models, which are prone to error. Results of LiDAR analyses depend heavily upon the density and quality of the initial LiDAR survey data points; however, additional data is not always more helpful in resolving individual features over larger areas. The spatial resolution used to identify depression was 0.5 m, so any features with a smaller diameter could not be resolved. Vertical accuracy also reduced confidence in mapping features with a depth less than 0.077 m.

Though karst features have been previously documented near developed areas, sinks were near-impossible to discern from anthropogenic depressions using remote sensing. The largest degree of error found in the random point survey stemmed from unidentified trails in highly vegetated areas. The network of major roads has changed very little over the past 10 years, as evidenced by satellite imagery. Minor roads and trails, however, are much more dynamic over short periods of time. The level of vehicle activity in western Fort Hood creates numerous depressions every year; in turn, the confidence in minor road filters

decreases with the age of the buffering polylines. Moreover, there are numerous trails that don't exist in any database and fail to show in satellite imagery.

Creating entirely inclusive trail filters in these types of areas requires significant effort; the smallest of minor roads cannot be accounted for without losing most of the efficiency this model offers. The filtering mechanisms used to remove natural phenomena were much more successful since areas with little to no development showed significantly improved accuracy. Underlying lithology is static and stream bodies change more slowly than the interval between LiDAR surveys.

Karst Potential and Edge Effect

Since its inception (Stafford et al., 2002), the GIS-based approach to sinkhole delineation has been implemented using increasingly precise LiDAR surveys. As spatial resolution in LiDAR surveys increase, so does the need for finer detail in filtering depressions. It is important to fully understand the relative magnitude of small-scale variations in lithology and topography when conducting remote sensing surveys, especially those involving karst. The prevalence of karst near ridges and escarpments proves particularly troublesome as these areas tend to host many sinks near the top of the plateaus within the Edwards Formation, but typically host little to no karst in the immediate lowlands. This

creates an edge effect when determining karst potential, where the neighborhood used in density maps may cause “hot spots” to bleed into areas that should not contain karst.

It is important to note that while karst potential is very useful in making generalized observations over large areas, the inventory of karst polygons can be used in many different capacities to locate new features. For instance, the neighborhood of 1 km, which was used in this study to capture regional trends without excluding localized concentrations of sinks, can be increased or decreased to better serve the needs of the user. Smaller neighborhoods are less useful in describing western Fort Hood as a whole but tend to suffer less from the edge effect mentioned previously. Figure 1.19 shows the differences that smaller neighborhoods make in determining localized karst potential.

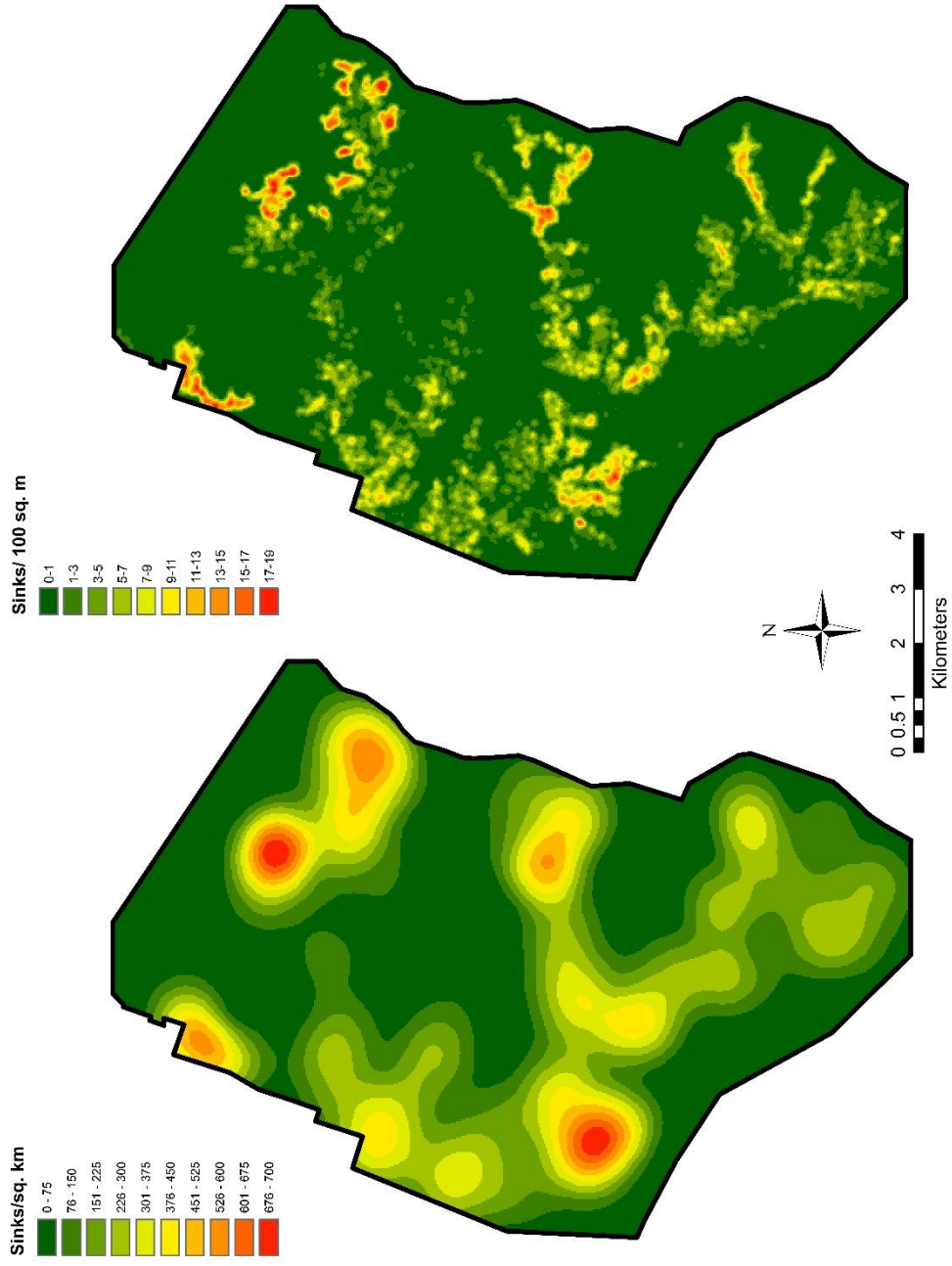


Figure 1.19: Comparison between karst potential models using 1 km neighborhood (left) and 100 m neighborhood (right).

CONCLUSIONS

The overall character of mapped and potential karst features found within this study support the initial observations of previous speleological surveys. Previous studies described a division between sinkholes related to the solutional widening of fractures and those more closely tied to bedrock collapse or suffosion processes (Faulkner, 2013; Reddell et al., 2011). Analyses of the lineament and morphology of potential sinks revealed that both mechanisms could contribute to sinkhole development in western Fort Hood. Karst are generally limited to areas of high elevation, where underlying lithology is the largest controlling factor. They also tend to form in clusters or roughly localized groups, due in part to the geomorphology of the plateaus.

LiDAR analysis was used to detect 13,969 potential sinks. The fill-difference method can be used to accurately and efficiently describe the distribution of karst over large areas. Previously mapped features in western Fort Hood show bias toward the most accessible areas; this model, instead, works best in undisturbed areas, where the origins of non-karst depressions are easier to predict. Roads, trails and other improvements throughout Fort Hood decrease confidence where they are most abundant. Western Fort Hood is primarily used in heavy equipment training, and thus required heavy filtering to reduce error. This may have removed potential karst from the survey, creating false negatives;

however, many of the karst features in heavily trafficked areas have already been recorded in previous studies and do not require remote sensing to detect. The resolution of the LiDAR survey also inhibited the detection of features smaller than 0.5 m or shallower than 8 cm. Accuracy assessment revealed that the survey was capable of accurately locating karst depressions 89% of the time; however, this model tends to overestimate the number of features. This is significantly reduced in areas with fewer variables that could explain the presence of depressions. The results of this survey will be used to directly aid the efforts of researchers at Fort Hood, primarily through the location and relocation of karst within their own database.

FUTURE WORK

The survey used in this study served to accurately define areas of karst development and susceptibility. Further study is required to measure the precise dimensions of the depressions and any associated subsurface passages within their extent. Furthermore, an updated collection of LiDAR data with even higher accuracy should be available within the next 10 years and could possibly delineate new features with greater confidence. Previous studies have indicated that many horizontal conduits exist beneath the surface at Fort Hood, some without navigable surficial expressions (Reddell et al., 2011; Veni, 1994). Since remote surveys are only useful in detecting surface phenomena, they cannot be used to characterize subsurface connectivity between features. This study should be used to target areas of high karst potential in geophysical surveys that can accurately resolve any solutional passages underground. Resistivity, in particular, is useful in mapping karst less than 10 m in depth (Majzoub, 2016; Zhou et al., 2002).

REFERENCES

- Adkins, W.S., and M.B. Arick, 1930, *Geology of Bell County, Texas*. The University of Texas Bulletin No. 3016, Austin: Bureau of Economic Geology.
- Amsbury, D.L., T.A. Jr. Bay, and F.E. Lozo, 1984, *A Field Guide to Lower Cretaceous Carbonate Strata in the Moffatt Mound Area near Lake Belton, Bell County, Texas*. Guidebook for SEPM Field Trip NO. 3. San Antonio: Gulf Coast Section of the Society of Economic Paleontologists and Mineralogists Foundation, 1-19.
- Anaya, R., and Jones, I., 2009, *Groundwater Availability Model for the Edwards-Trinity (Plateau) and Pecos Valley Aquifers of Texas*. Report 373, Texas Water Development Board, 103 p.
- Angel, J.C., Nelson, D.O. and Panno, S.V., 2004, *Comparison of a new GIS-Based Technique and a Manual Method for Determining Sinkhole Density: An Example from Illinois' Sinkhole Plain*, Journal of Cave and Karst Studies, vol. 66, no. 1, p. 9-17.
- Bryant, A.W., 2012, *Geologic and Hydrogeologic Characterization of Groundwater Resources in the Fredericksburg Group, North Nolan Creek Province, Bell County, Texas*. Master's Thesis, Nacogdoches: Stephen F. Austin State University.
- Elliott, W.R., and Veni, G., 1994, *The Caves and Karst of Texas*, Convention of the National Speleological Society, 1994 guidebook: National Speleological Society and Texas Parks and Wildlife Department, p. 26-28.
- ESRI, 2018, *ArcGIS Desktop 10 Resource Center*.
<https://support.esri.com/en/Products/Desktop/arcgis-desktop> (first accessed March 2018)
- Faulkner, M.G., 2016, *An Investigation of Hydrogeologic, Stratigraphic, and Structural Controls on Acer Grandidentatum Communities in a Karst*

Landscape, Owl Mountain Province, Fort Hood Military Installation, Texas.
Dissertation, Nacogdoches: Stephen F. Austin State University.

- Faulkner, M.G., Stafford, K.W. and Bryant, A.B., 2013, *Delineation and Classification of Karst Depressions Using LiDAR: Fort Hood Military Installation, Texas*, NCKRI Symposium 2: Proceedings of the 13th Multidisciplinary Conference on Sinkholes and the Engineering and Environmental Impacts of Karst. Carlsbad, NM: National Cave and Karst Research Institute.
- Ferrill, D.A., and Morris, A.P., 2008, *Fault Zone Deformation Controlled by Carbonate Mechanical Stratigraphy, Balcones Fault System, Texas*: American Association of Petroleum Geologists Bulletin, v. 92, no. 3, pp. 359-380
- Fisher, W.L., and Rodda, P.U., 1969, *Edwards Formation (Lower Cretaceous), Texas: Dolomitization in a Carbonate Platform System*. American Association of Petroleum Geologists 53, no. 1: p 55-72.
- Flood, Flood, M., 2004, *ASPRS Guidelines Vertical Accuracy Reporting for LiDAR Data*, ASPRS, p. 1-20.
- Gutierrez, F., Guerrero, J. and Lucha, P., 2008, *A Genetic Classification of Sinkholes Illustrated from Evaporite Paleokarst Exposures in Spain*, Environmental Geology, vol. 53, p. 993-1006.
- Hammer, M.L., 2011, *Introduction and Site Description, in Endangered Species Monitoring and Management at Fort Hood, Texas*. Fort Hood: Fort Hood, Directorate of Public Works, Natural Resources Management Branch.
- Hayward, O.T., Allen, P., Amsbury, D., 1990, *The Lampasas Cut Plain: Evidence for the Cyclic Evolution of a Regional Landscape, Central Texas*. Guidebook for Geological Society of America Field Trip No. 19, Geological Society of America, 113 p.
- Hu, Y., 2003, *Automated extraction of digital terrain models, roads and buildings using airborne LiDAR data*, University of Calgary, Department of Geomatics Engineering, pp. 85-88.

- Klimchouk, A.B., 2007, *Hypogene Speleogenesis: Hydrogeological and Morphogenetic Perspective*. Special Paper no.1, National Cave and Karst Research Institute, Carlsbad, NM, 106 pp.
- Klimchouk, A.B., 2009, *Principal Characteristics of Hypogene Speleogenesis, in Advance in Hypogene Speleogenesis, Symposium 1*, National Cave and Karst Research Institute, p. 1-11.
- Kobal M., Bertonec I., Pirotti F., Dakskobler I. and Kutnar L., 2015, *Using Lidar Data to Analyze Sinkhole Characteristics Relevant for Understory Vegetation Under Forest Cover—Case Study of a High Karst Area in the Dinaric Mountains*, PLOS One, vol. 10, no. 3, p. 1-19.
- Majzoub, A., 2016, *Characterization and Delineation of Karst Geohazards Along RM652 Using Electrical Resistivity Tomography, Culberson County, Texas*. Master's Thesis, Nacogdoches: Stephen F. Austin State University.
- Nelson, H.F., 1973, *The Edwards Reef Complex and Associated Sedimentation*, The Geological Society of America, Dallas, Bureau of Economic Geology, 1-35.
- Optimal Geomatics, 2009, *LiDAR Data Processing Procedures Report*, Optimal Geomatics Inc., p. 5.
- Pettorelli, N., Vik, O. J., Mysterud, A., Gaillard, J., Tucker, C. J. and Stenseth, N., 2005, *Using Satellite-Derived NDVI to Assess Ecological Responses to Environmental Change*, Trends in Ecology and Evolution, vol. 20, no. 9, p. 503-510.
- Pugsley, W S., 2001, *Imprint on the Land, Life Before Camp Hood, 1820-1942*,. Prewitt and Associates.
- Quantum Spatial, 2015, *Field Survey Report of Photo ID Ground Control Points*, Quantum Spatial Inc.
- Reddell, J.R., Fant, J., Reyes, M., and Warton, M., 2011, *Karst Research on Fort Hood, Bell and Coryell Counties, Texas*. Unpublished Report, Fort Hood: Fort Hood Natural Resources Management Branch.

- Rose, P.R., 1972. *Edwards Group, Surface and Subsurface, Central Texas*, Report of Investigations, no. 74, Bureau of Economic Geology, 198 p.
- Scholle, P.A., Bebout, D.G., Moore, C.H., 1983, *Carbonate Depositional Environments: AAPG Memoir 33*. American Association of Petroleum Geologists, vol. 33, 708 p.
- Stafford, K.W., Rosales-Lagarde, L., Boston, P.J., 2002, *Castile Evaporite Karst Potential Map of the Gypsum Plain, Eddy County, New Mexico and Culberson County, Texas: A GIS Methodological Comparison*, Journal of Cave and Karst Studies, vol. 70, no. 1, p. 35-46.
- Stehman, S. V., 1997, *Selecting and Interpreting Measures of Thematic Classification Accuracy*, Remote Sensing of Environment, vol. 62, no. 1, p. 77-89
- Stricklin, F.L., Smith, C.I., and Lozo, F.E., 1971, *Stratigraphy of Lower Cretaceous Trinity Deposits of Central Texas*, Report of Investigations, no. 71, Bureau of Economic Geology, 63 p.
- Talbert, S. J., Atchley, S.C., 2000, *Sequence Stratigraphy of the Lower Cretaceous (Albian) Fredericksburg Group, Central and North Texas*. Gulf Coast Association of Geological Societies Transactions, vol. 50, p. 369-377.
- Veni, G., 1994, *Hydrogeology and Evolution of Caves and Karst in the Southwestern Edwards Plateau, Texas*. The Caves and Karst of Texas, National Speleological Society, Huntsville, Alabama. 252 pp.
- Walker, L.E., 1979, *Occurrence, Availability, and Chemical Quality of Ground Water in the Edwards Plateau Region of Texas*, Report 235, Texas Department of Water Resources, 336 p.
- Wang, L. and Liu, H., 2006, *An Efficient Method for Identifying and Filling Surface Depressions in Digital Elevation Models for Hydrologic Analysis Modeling*, International Journal of Geographic Information Science, vol. 20, no. 2, p. 193-213.

Wu, Q., Deng, C. and Chen, Z., 2016, *Automated Delineation of Karst Sinkholes from LiDAR-Derived Digital Elevation Models*, *Geomorphology*, vol. 226, p. 1-10.

Zhou, W., Beck, B., and Adams, A., 2002, *Effective Electrode Array in Mapping Karst Hazards in Electrical Resistivity Tomography*. *Environmental Geology*, vol. 42, p. 922–928.

APPENDIX

DETAILED METHODOLOGY

KARST SURVEY

Sinkholes were derived from LiDAR survey and configured into filtered and classified shapefiles in three major steps: (1) LiDAR processing, (2) depression extraction, and (3) depression classification. Data was sourced from the Texas Natural Resource Information System, the Bureau of Economic Geology, the Fort Hood Natural Resources Division, Quantum Spatial Inc., and Google Earth Satellite Imagery. LiDAR processing was completed using in ESRI's ArcMap 10.5. This study follows the "fill-difference" model outlined in other recent karst surveys (Doctor & Young, 2013; Faulkner et al., 2013; Bryant, 2012). Sinkholes in the study area are generally smaller than 5m in diameter, and the study area contains numerous fluvial and man-made depressions.

Potential sinkholes required significant filtering to make sure that all sinkholes considered for this study met five criteria: (1) underlying lithology must be either Comanche Peak or Edwards as the Walnut Formation does not have the potential to host karst; (2) sinks should not be immediately proximal to roads or trails; (3) sinks should not intersect fluvial drainage areas or any other water bodies; (4) sinks should not be located on bare ground surfaces near any land improvements, as non-vegetated areas in the open are almost always impacted by military activity; (5) the lowest point should be greater in depth than the vertical accuracy of the survey to reduce false positives.

LIDAR & DEM PROCESSING

LiDAR Survey

Quantum Spatial was contracted by the U.S Army Corps of Engineers to conduct airborne LiDAR surveys in March of 2015. Data was collected in 48 flight lines with 70 accuracy control points that covered an 880 km² area over Fort Hood. Data was processed and classified by values for GPS location, pitch, roll and heading from the plane's onboard POS (Positioning Orientation System) (Quantum Spatial, 2015). Ground control points were set at five locations and used to test the positional accuracy of the raw LiDAR data. Statistics were calculated from known ground control points and their respective laser returns, with a RMSE_(z) of 0.039 m. Vertical accuracy in a LiDAR survey should be 1.96 times greater than RMSE(z), giving 95% confidence in a vertical accuracy of 7.7 cm over the study area (Flood, 2004; Quantum Spatial, 2015). Horizontal point spacing for the ALS70 sensor has been measured at 30 cm for 4300 feet flight altitude (7850 feet in this survey); therefore, it was determined that the expected horizontal spacing was less than 0.55 m for this survey (Quantum Spatial, 2015). LAS files were created and classified by Quantum Spatial to isolate points with

laser returns from ground, vegetation and other surface features. LAS datasets were acquired from the Natural Resource Division at Fort Hood.

DEM Processing

LAS files were converted to multipoint features using the *LAS to Multipoint* tool in ArcMap. Parameters were chosen such that only the last return from classes 0 (never classified), 1 (unidentified), 2 (ground) and 8 (key markers) were kept for further analysis. This ensures that vegetation is not modeled as terrain, which is crucial in these surveys. The high density and accuracy of LiDAR data lends itself to storage and memory limitations, so a digital terrain model (DTM) was created to simplify data points. The terrain model was constructed using the *Create New Terrain Wizard* and populated with multipoint files (mass points) containing the elevation data and digitized polylines which represented breaklines in the LiDAR survey. The point spacing used for this new model was 0.52 m; this represents a calculated average of the point spacing in all of the multipoint files. The *Terrain to Raster* tool was then used to convert the vector-based DTM into a format that could handle cell-based calculations. The natural neighbor method was chosen for interpolation because it creates a smoother and more accurate model than similar methods (ESRI, 2018). Cell size (i.e. resolution) was determined using:

$$S = \sqrt{\frac{A}{n}} \text{ (Equation 2.1)}$$

Where S is the grid size, n is the total number of data points and A is the area of the DEM (Hu, 2003). This means that grid size should approximate the point spacing of the original survey. The resulting 0.5 m DEM (digital elevation model) allowed detailed spatial analysis of the relationship between cells, specifically using the *Hydrology* toolset under the *Spatial Analyst* toolbox (Figure 2.1). This process is outlined in figure 2.2, which shows each step taken from LAS files to DEM creation.

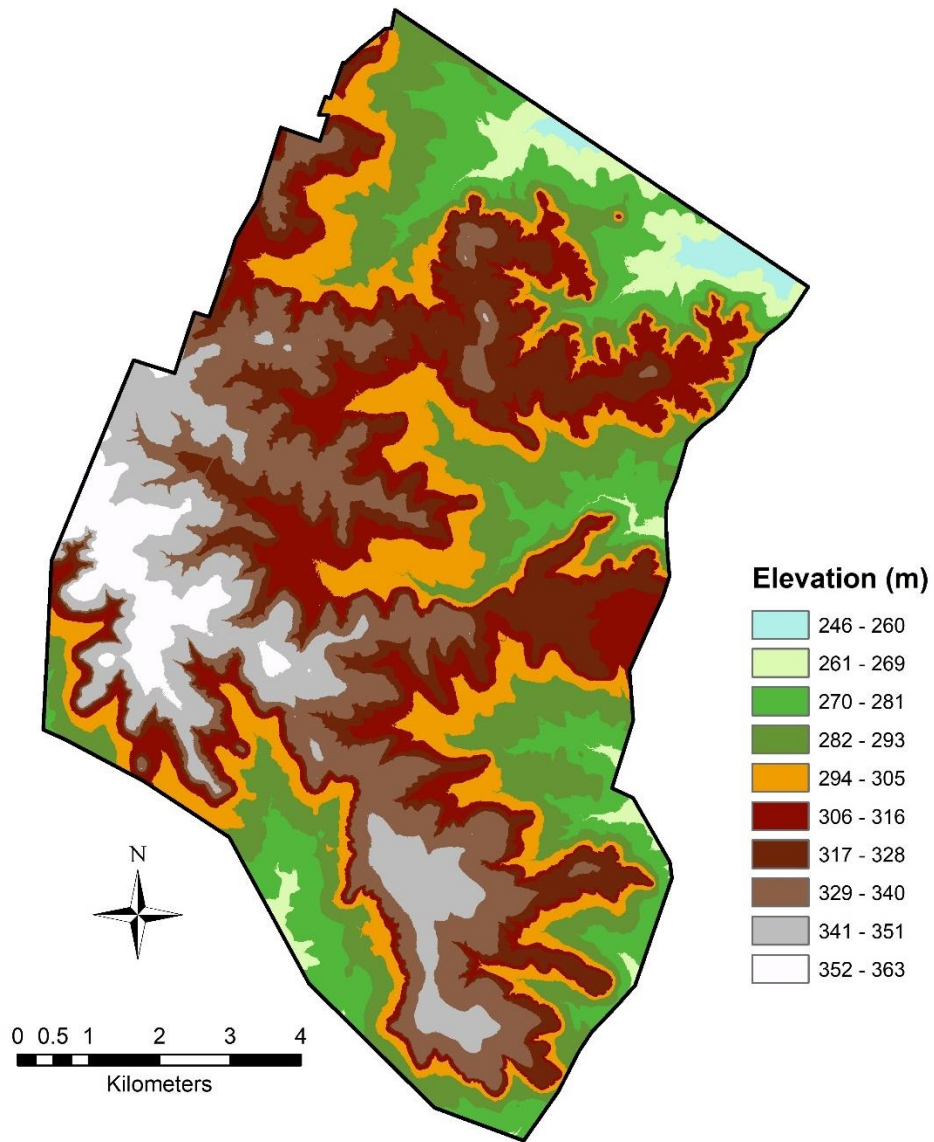


Figure 2.1: 0.5 m digital elevation model created to characterize the landscape of Fort Hood.

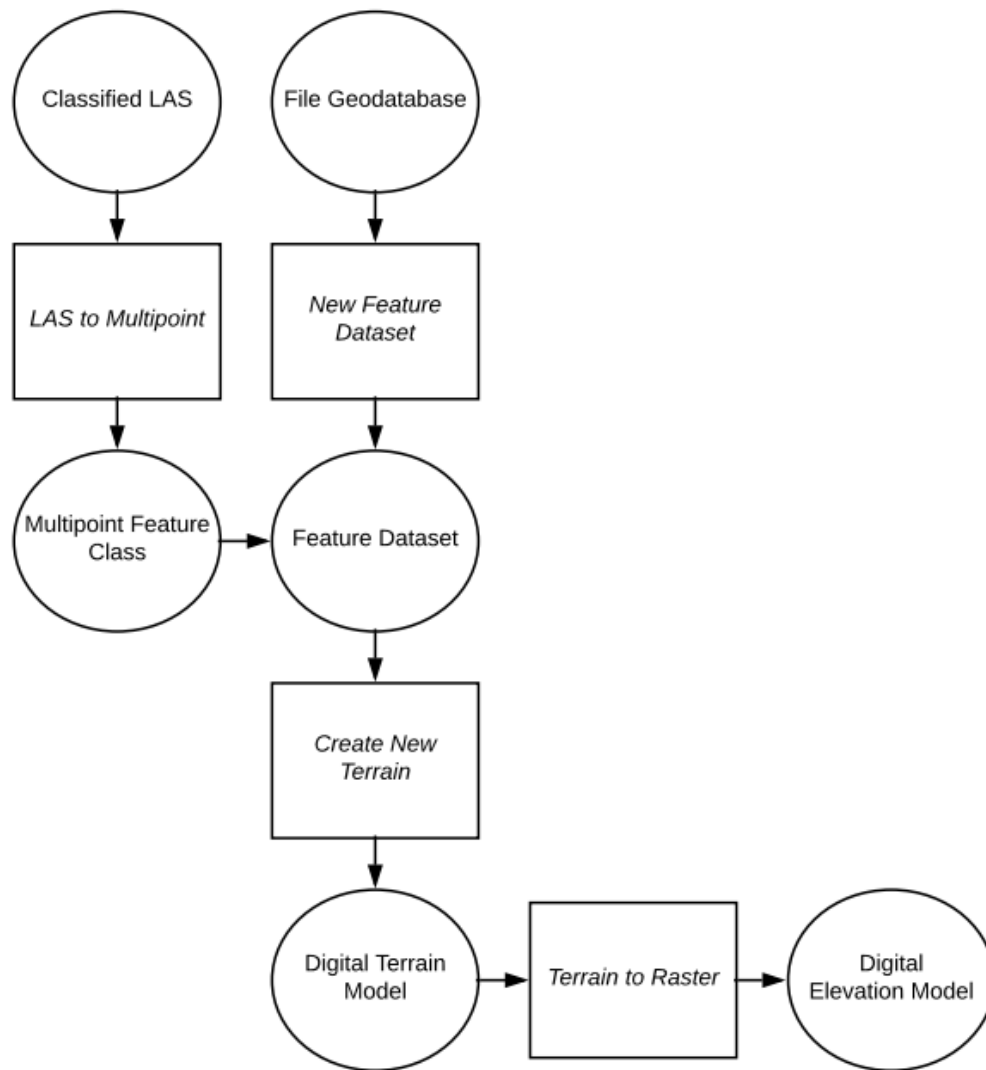


Figure 2.2: Flow diagram representing the required processes in the creation of DEM from LAS files.

DEPRESSION IDENTIFICATION

Depressions can be detected from digital elevation models in several ways. Early studies used models that measured relative position to find negative anomalies by creating a TPI (topographic position index) raster or calculating slope. These models lack spatial context, however, and required extensive subjective filtering by the user. They also work best in raster models with very low elevation tolerances (i.e. low relief), and thus would not be suited to characterize the study area (Angel et al., 2004; Wang & Liu, 2006). Sinkholes are best treated as hydrologic anomalies rather than topographic anomalies, where connectivity to other areas of flow accumulation is taken into consideration (Stafford et al., 2002; Kobal et al., 2014). The emergent fill-difference method outlined in this section uses an inclusive tool that was originally designed to reduce surface complexity to extract features with a pour point. Pour point defines the height of watershed above an isolated depression and is often referred to as the spill elevation (Wang & Liu, 2006). The *Fill* tool uses an iterative process that determines flow direction and finds areas where a direction does not exist. It then fills that cell to its pour point to correct the flow direction and repeats this process until there are no “sinks” left in the raster (ESRI, 2018). The resulting DEM has the same values as the original raster in all locations

except those with sinks, where the value is raised to effectively remove the depression.

After depressions were filled to their pour point, they were extracted using *Raster Calculator* to subtract values in the original DEM from those in the newly-filled DEM. The fill-difference (or “minus”) raster showed only values for the calculated depth of depressions as all other values were reduced to zero. Using the *Set Null* tool, these zero values were removed from the raster to isolate depressions from the background. *Raster Calculator* and *Int* (float to integer conversion tool) were then used to convert meters to centimeters and remove decimals from the raster values. *Raster to Polygon* was used to convert the image from raster to feature class and measure the spatial attributes of each depression. This tool requires that raster values be in integer form, thus necessitating the previous step. Depression polygons were then redefined by dissolving boundaries between cells and simplifying the shape of discrete features. Figure 2.3 represents the processes used to extract depressions from a DEM and convert them to polygons.

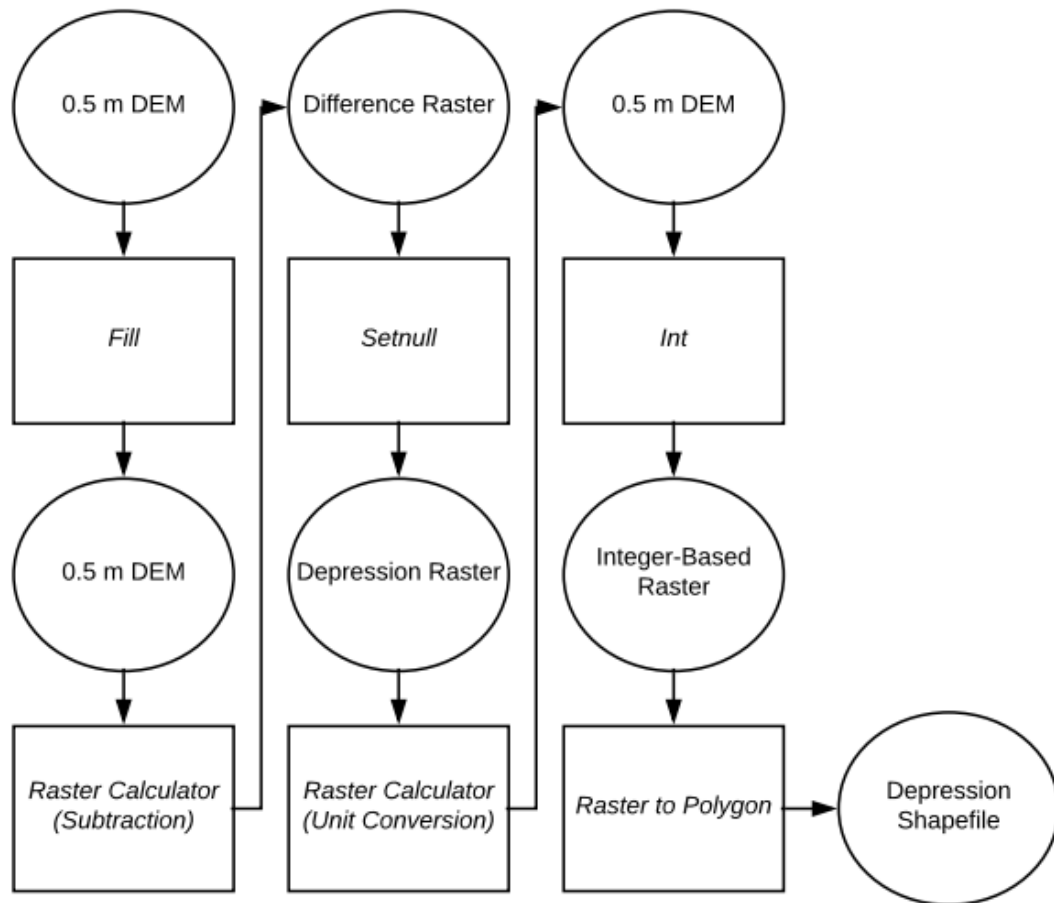


Figure 2.3: Flow diagram representing the sequence of processes required to extract depressions from a 0.5 m DEM into a polygon shapefile.

DEPRESSION CLASSIFICATION

The method described above identifies all depressions within the extent of the DEM. The vast majority of these features are not karst-derived, but rather controlled by anthropogenic and geomorphological processes which form false positives that may be mistaken for sinkholes. Depressions must be filtered and classified by their spatial relationships with other existing features such as roads, streams and other water bodies. Furthermore, the underlying geology should be susceptible to dissolution and localized topographic relief (cliffs, incised valleys, etc.) should not exist nearby. Most of the depressions found in this study had depths less than 1 m; however, potential sinkholes with a depth that did not exceed the vertical accuracy of the LiDAR survey could not be considered due to the lack of confidence.

Depressions in proximity to roads and other developed areas were removed first, using manually delineated features and land cover types. Major roads transect the entire study area, and are usually accompanied by engineered drainage and internal depressions. Aerial imagery was used to digitize the centerline of all major roads; most were constructed with two lanes and divided at the center (Figure 2.4). A buffer zone of 15 m (originally 20 m) was then applied

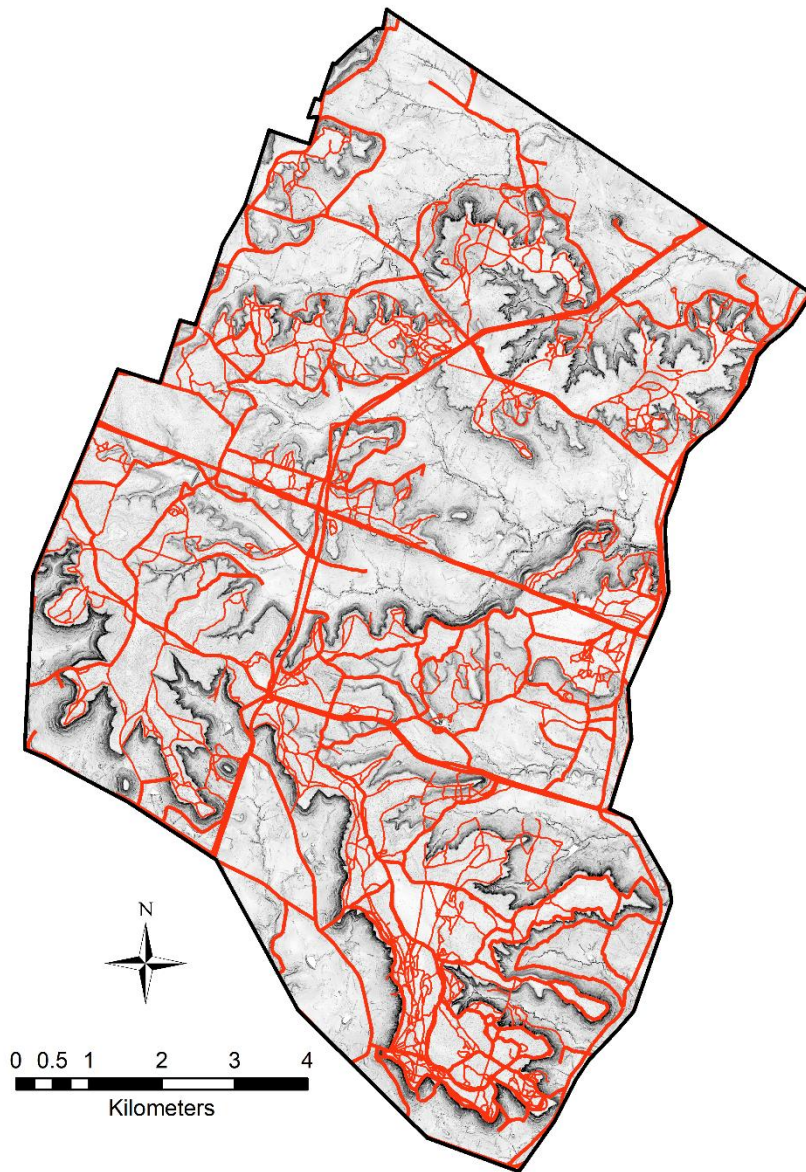


Figure 2.4: Major and minor roads delineated using an existing database and satellite imagery.

to the road polylines to incorporate nearby ditches and culverts. Minor roads consist of trails, tank roads and smaller byways connecting the major roads. Their width is almost never greater than 5 m and the associated drainage areas are less pronounced. These roads were digitized and given a 10 m buffer from the centerline to incorporate only the immediate trail areas. Training sites, unpaved lots and other developed areas were delineated by measuring the spectral intensity of the land surface. Intensity is a measure of the amount of light that is reflected from an object at the surface. Light is represented by a spectrum of different wavelengths and categorized by ranges within that spectrum. Intensity is often collected in several bands representing each different wavelength and recorded for each cell with a value between 0 and 255. NDVI (Normalized Difference Vegetation Index) is commonly used to distinguish land cover classes and is calculated by:

$$NDVI = \frac{(NIR-Red)}{(NIR+Red)} \text{ (Equation 2.2)}$$

where “NIR” and “Red” represent the intensity their respective wavelength within each cell (Pettorelli et al., 2005). The *NDVI* function of the *Image Analysis* window was used to produce a land cover map. Areas designated as “developed” or “bare-ground” were used to filter and remove depressions (Figure 2.5).

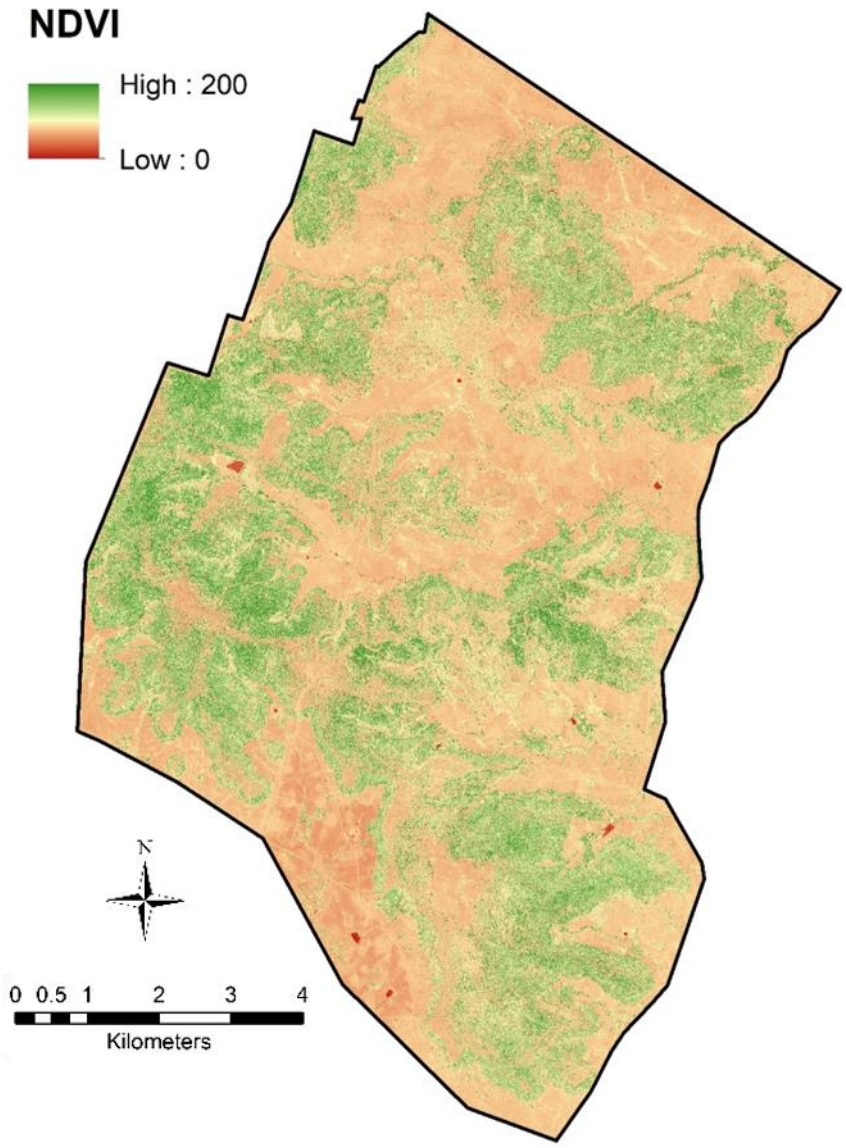


Figure 2.5: A normalized difference vegetation index colormap representing different land cover types within the study area. Cover types designated as “bare” or “developed” were used for removal.

Streams, rivers and ponds were delineated to remove natural depressions that are not related to karst processes. Water bodies naturally incise the landscape, forming anomalous lows in streambeds that can appear as isolated sinks. Ponds were manually digitized and buffered to include 20 m of the immediately surrounding area. Streams were delineated using a flow accumulation raster. Flow accumulation measures the accumulated weight of all cells flowing into a cell of lower elevation. Areas of the high concentrated flow (over 100,000 contributing cells) were to map streams and form a network of interconnected high-accumulation cells (Figure 2.6; ESRI, 2018). Streams were given a 5 m buffer from their centerline to include only the immediate drainage path.

Depressions were then classified by their underlying lithology using a geologic map. Any potential sinkholes in the area that do not overly the hydrologically sensitive Edwards or Comanche Peak Formations are not karst-related. A geologic map was acquired and modified from the Bureau of Economic Geology through the Texas Natural Resources Information System and applied as a filter to remove depressions overlying the Walnut and Glen Rose Formations (Figure 2.7). The depth of each depression was compared to the vertical accuracy of the LiDAR survey, which was calculated as 0.37 m. Any depressions whose depth did not exceed the vertical accuracy had to be

dismissed from further evaluation. Though some shallow sinkholes were likely removed from the study during this step, those depressions simply could not be accurately resolved using this model. The filtering process used in depression classification is outlined in figure 2.8.

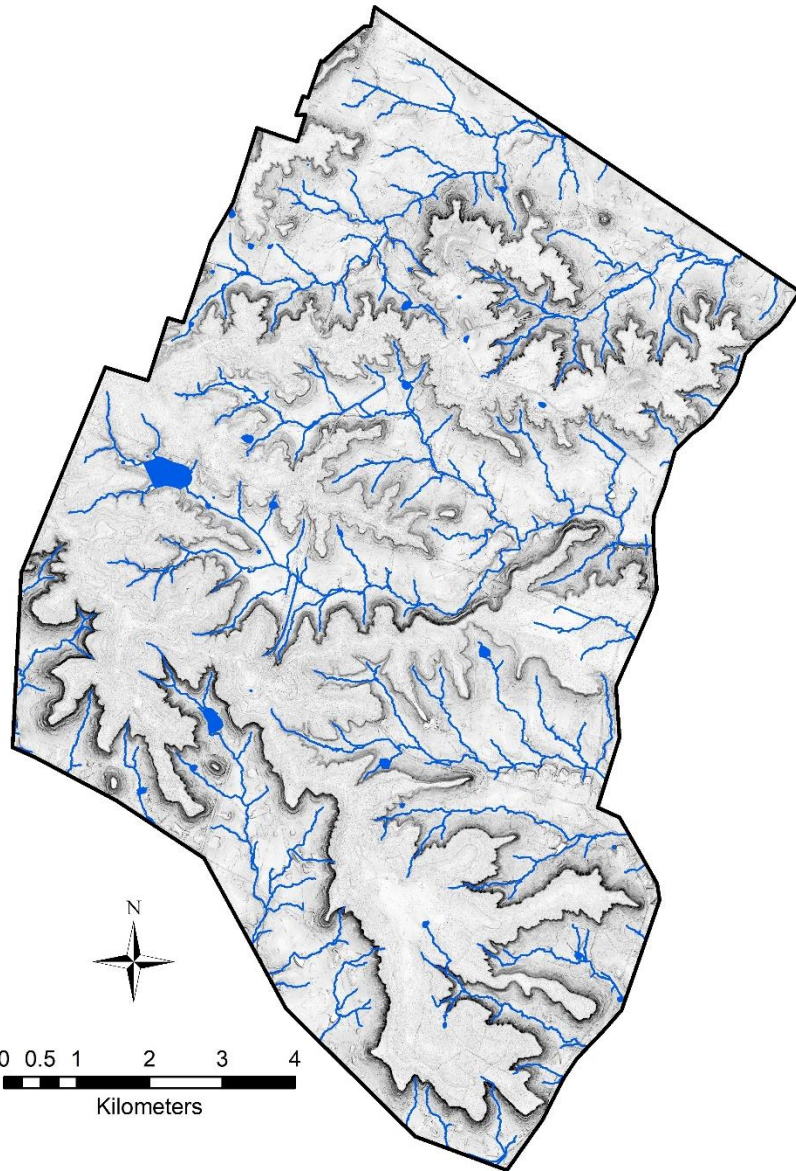


Figure 2.6: Stream networks and ponds delineated using the *Flow Accumulation* tool and aerial imagery from the LiDAR survey data package.

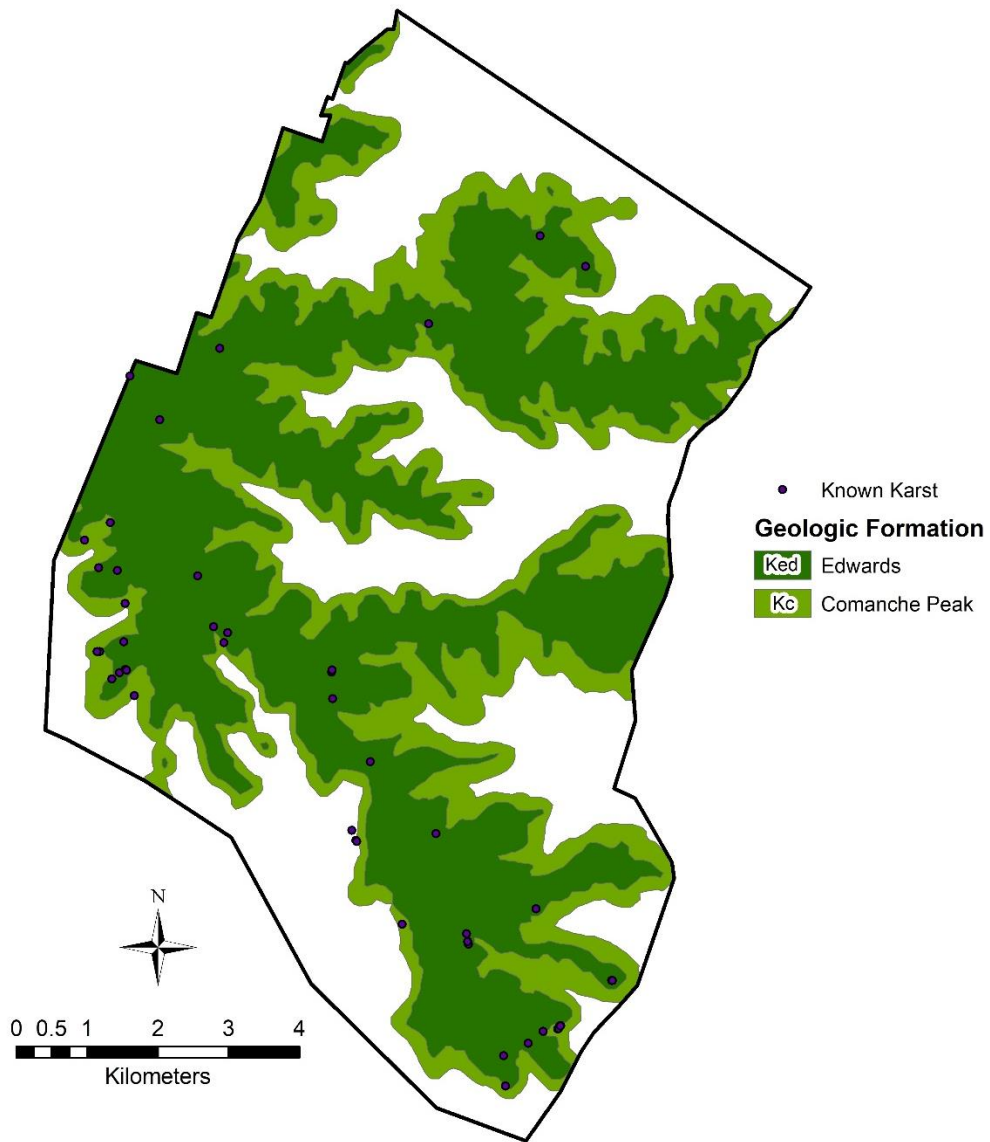


Figure 2.7: Geologic map of the study area showing only the units susceptible to karst. Note that every known karst feature lies within these two units.

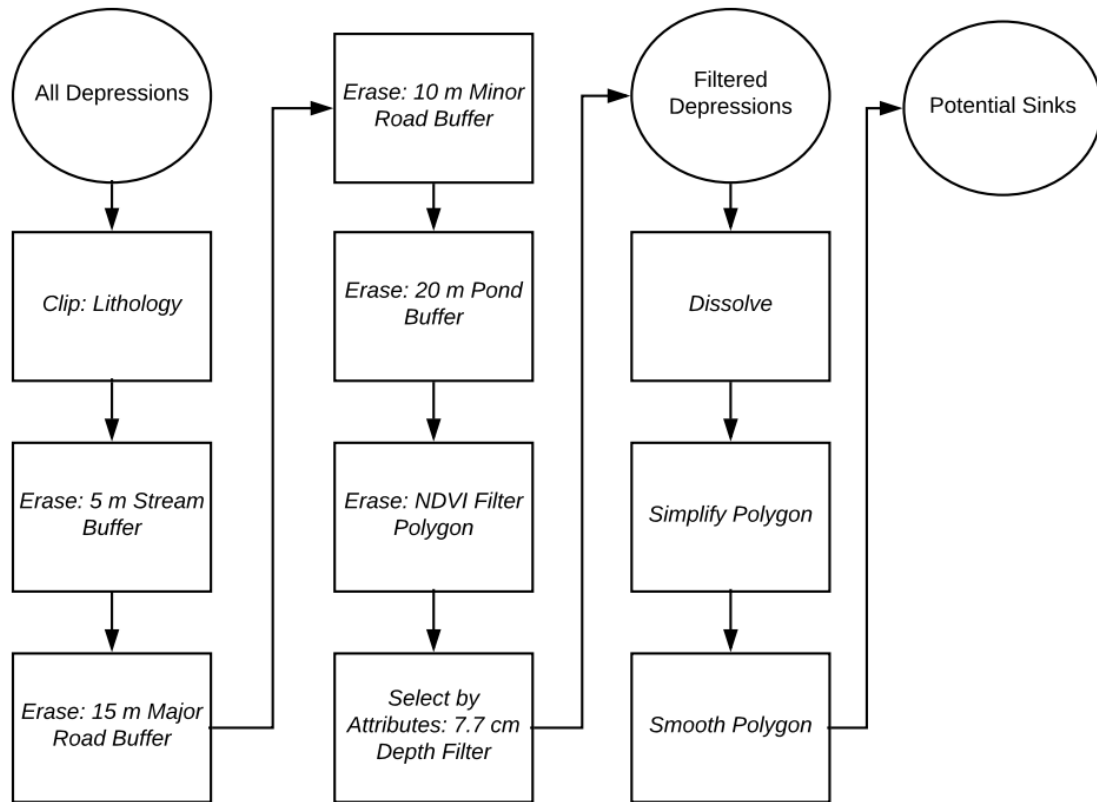


Figure 2.8: Flow diagram of the filtering processes used to delineate potential sinks and classify them by their spatial attributes.

DEPRESSION ANALYSIS

Karst Potential

While an inventory of depression polygons is useful in characterizing individual features, the inherent limitations of LiDAR surveys create at least some false positives and negatives. A more useful way to interpret the large-scale distribution of sinks is by creating a karst potential model. Karst potential is a generalized concentration of karst-related depressions in an area. The *Kernel Density* tool was used to determine which areas contained the most significant karst manifestations. Polygons were converted to individual points and used to produce two raster models: the first measured the number of features in a neighborhood of 1 km², while the second measured the surface area of features using the same neighborhood of 1 km².

The point density model showed the greatest concentrations at areas of high elevation, particularly at the western border of Fort Hood where the Shell Mountain Plateau peaks in elevation (Figure 2.9). An additional area-density model was created to better represent the magnitude of the sinks in an area (Figure 2.10). Point density takes an unbiased account of the occurrences in an

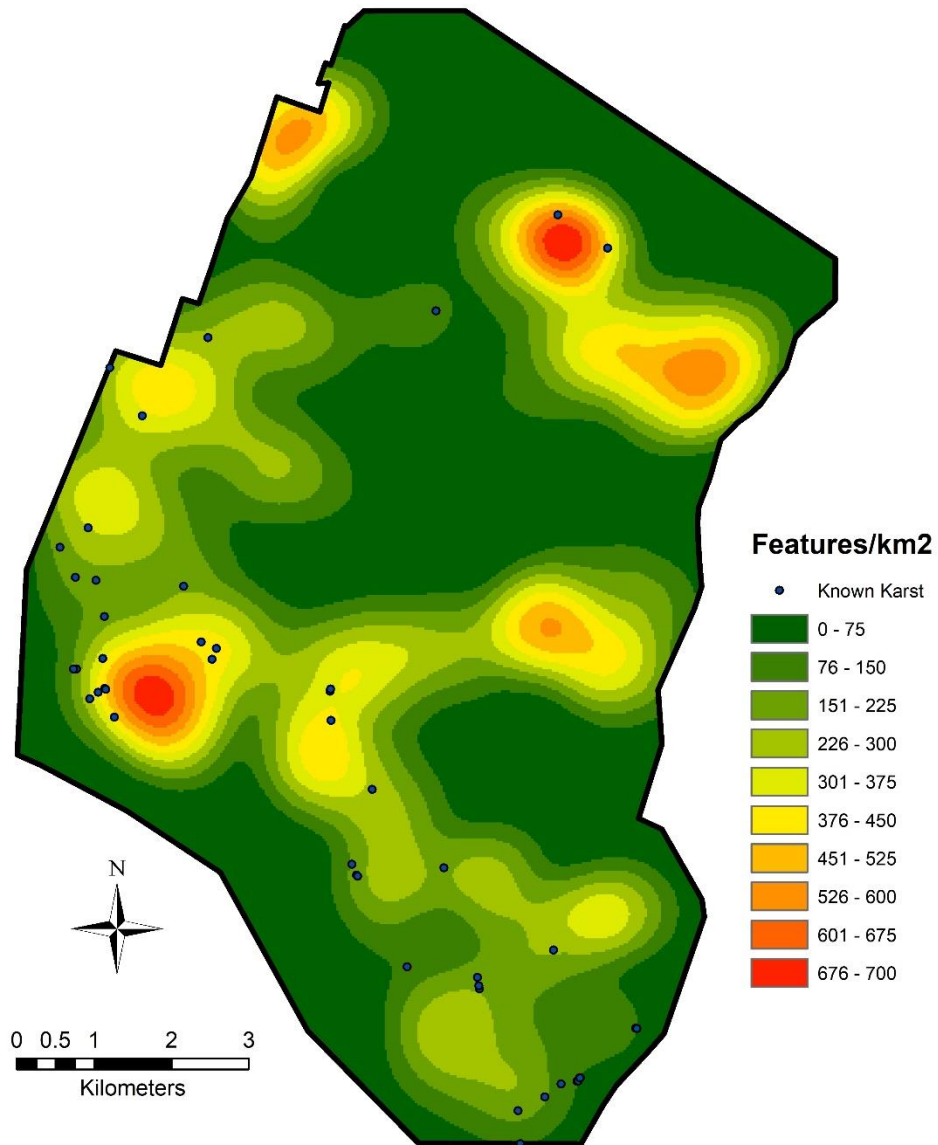


Figure 2.9: Point density map of non-interfering depressions in the survey.

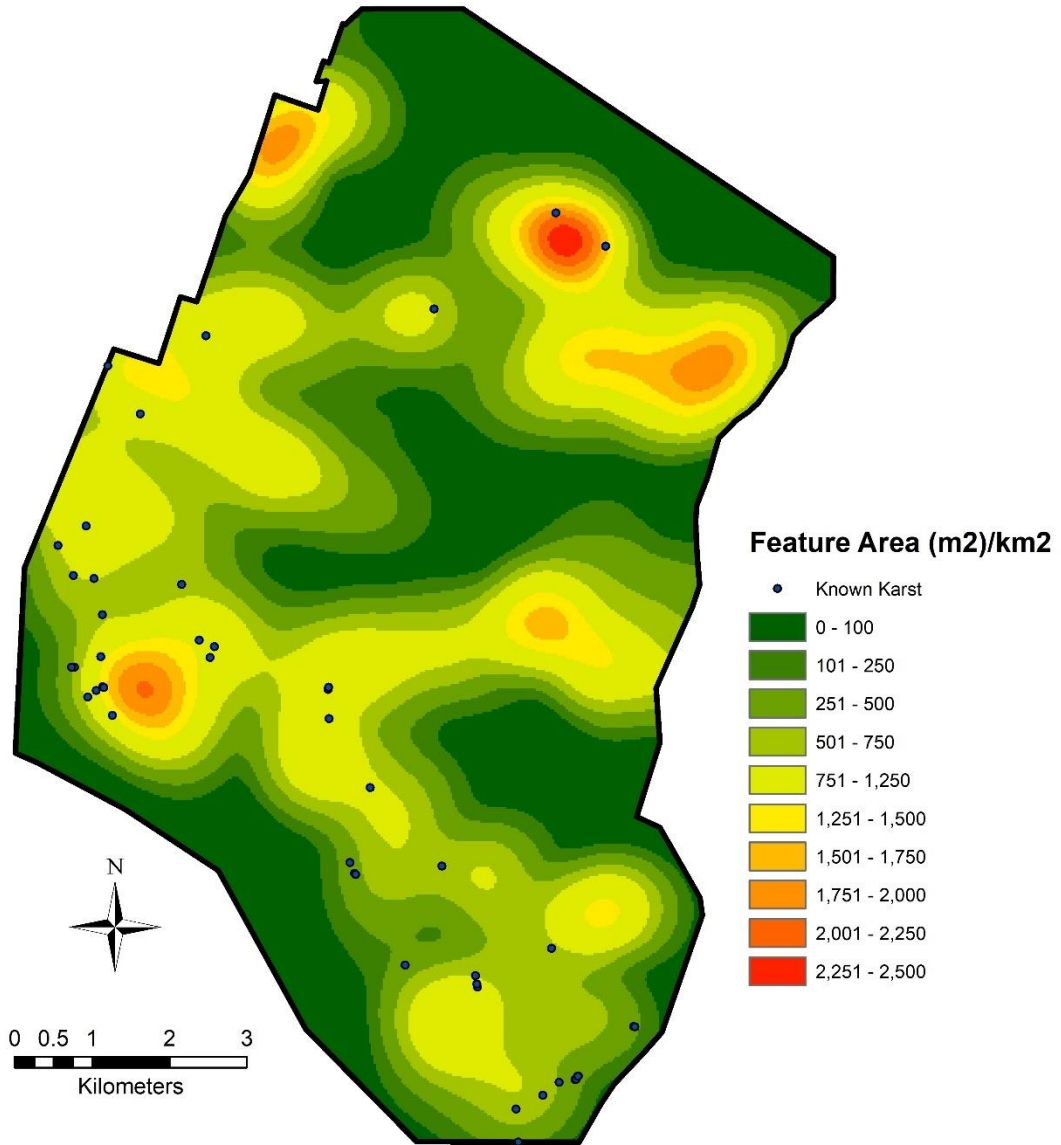


Figure 2.10: Area density map showing the magnitude of concentrated features per km².

area, which can mislead interpretations when most features are closer in size to karren (in the form of pits or potholes) than sinkholes. The distribution of sinks in both models supports the initial observation that karst are relatively clustered in pockets of soluble rock within the study area. More importantly, the density of karst in this survey does not match the density of previously mapped features; this exemplifies the disconnection between what is surveyed and what likely exists at the surface.

Morphology & Lineament

Non-interfering sinkholes were further classified by their circularity to characterize the relative stage of development through degree of collapse. This provided a way to gather statistics on the shapes of depressions and, to a lesser extent, describe the accuracy of delineated sinks. The ratio of length (major axis) to width (minor axis) should be 1:1 in a perfect circle and should not exceed 2:1 in karst features, which tend to be less elliptical than other depressions ().

Dimensions were calculated for each potential sinkhole using the *Minimum Bounding Geometry* tool to create rectangles with more easily measurable dimensions. The values were put into a table in *Microsoft Excel* and graphed using length in the x-axis and width in the y-axis. Two lines were created with a slope of 1 and 2 to represent circular and elliptical shapes respectively; any points that fell between these two have morphology similar to most sinkholes. A

linear trend was created for the dataset, showing an average circularity ratio of 1.31. Not only are most potential sinks within acceptable parameters, but they also trend toward a more circular habit than elliptical. This supports previous observations regarding the middle to late-stage development of collapse features in the region.

Minimum Bounding Geometry also recorded the orientation of the long axis in each depression. These orientations were classified by the azimuthal direction with values ranging from 0-180 degrees. The values were condensed into a single column in Microsoft Excel and exported to the Geo Orient Software package, which was used to display the data in a more spatially meaningful way. The lineament of each depression was added to a rose diagram in order to display trends found within the dataset (Figure 1.13). The average of these values is approximately 31 degrees, and many of the potential sinks exhibited a NE-SW trend. This is consistent with fractures and joint associated with Balcones deformation. Previous lineament analyses in eastern Fort Hood revealed a similar trend in the linear directions of both joints and sinkholes; the study suggested that the trend exists due to the relationship between dissolution and fracture porosity (Faulkner, 2016).

VITA

Colby B. Reece graduated from Ellison High School in Killeen, Texas. In December 2015, Colby graduated from the University of Houston where he received his Bachelor of Science in Geology. In January of 2017, he was admitted to the Graduate School of Stephen F. Austin State University and began pursuing his Master of Science in Geology. Colby received his Master of Science degree in December of 2018.

Permanent Address: 881 Cactus Circle
 Killeen, TX 76542

Style manual designation: Geological Society of America

This thesis was typed by Colby B. Reece